Developmental Biology 433 (2018) 416–432

Contents lists available at ScienceDirect

Developmental Biology

journal homepage: www.elsevier.com/locate/developmentalbiology

Original research article

Dynamics of actinotrichia regeneration in the adult zebrafish fin

Désirée König, Lionel Page, Bérénice Chassot, Anna Jaźwińska*

Department of Biology, University of Fribourg, Chemin du Musée 10, 1700 Fribourg, Switzerland

ARTICLE INFO

Keywords:
Actinodin
Blastema
Lepidotrichia
Wound epithelium
Osteoblasts
Extracellular matrix

ABSTRACT

The skeleton of adult zebrafish fins comprises lepidotrichia, which are dermal bones of the rays, and actinotrichia, which are non-mineralized spicules at the distal margin of the appendage. Little is known about the regenerative dynamics of the actinotrichia-specific structural proteins called Actinodins. Here, we used immunofluorescence analysis to determine the contribution of two paralogous Actinodin proteins, And1/2, in regenerating fins. Both proteins were detected in the secretory organelles in the mesenchymal cells of the blastema, but only And1 was detected in the epithelial cells of the wound epithelium. The analysis of whole mount fins throughout the entire regenerative process and longitudinal sections revealed that And1-positive fibers are complementary to the lepidotrichia. The analysis of *another longfin* fish, a gain-of-function mutation in the potassium channel *kcnk5b*, revealed that the long-fin phenotype is associated with an extended size of actinotrichia during homeostasis and regeneration. Finally, we investigated the role of several signaling pathways in actinotrichia formation and maintenance. This revealed that the pulse-inhibition of either TGFβ/Activin-βA or FGF are sufficient to impair deposition of Actinodin during regeneration. Thus, the dynamic turnover of Actinodin during fin regeneration is regulated by multiple factors, including the osteoblasts, growth rate in a potassium channel mutant, and instructive signaling networks between the epithelium and the blastema of the regenerating fin.

1. Introduction

The zebrafish caudal fin provides a valuable model system to study mechanisms of adult organ regeneration in vertebrates. After fin amputation, the zebrafish is able to swim and to restore the original size and shape of the appendage within approximately three weeks. This phenomenon depends on appropriate wound healing, creation of blastema progenitor cells and on their progressive redifferentiation, as recently reviewed (Jazwinska and Sallin, 2016; Tornini and Poss, 2014; Wehner and Weidinger, 2015).

The fin is a non-muscularized flattened appendage, which is used for propulsion while swimming. As opposed to the tetrapod limb, which is entirely supported by the endoskeleton, the fin fold is stabilized by skeletal elements of dermal origin, called rays, whereas the endoskeleton is confined only to the base of the fin (Grandel and Schulte-Merker, 1998; Thorogood, 1991; Witten and Huysseune, 2007). The zebrafish caudal fin typically contains 16–18 main occasionally bifurcated rays, which are connected by soft interray tissue (Akimenko et al., 2003; Mari-Beffa and Murciano, 2010; Pfefferli and Jaźwińska, 2015). Each ray contains a pair of segmented parenthesis-shaped bones, called lepidotrichia, which are deposited by osteoblasts underneath the stratified epidermis. The tips of the rays lack bones and are solely supported by unsegmented brush-like spicules, named actinotrichia (Becerra et al., 1983; Witten and Huysseune, 2007). While lepidotrichia are dermal structures, actinotrichia are considered to be of ectodermal origin, as they are formed in the early embryonic fin fold, before mesenchyme recruitment, and they precede the differentiation of rays in various fish species (Dane and Tucker, 1985; Feitosa et al., 2012; Geraudie, 1977; Grandel and Schulte-Merker, 1998; Heude et al., 2014; Kemp and Park, 1970; Thorogood, 1991; Wood and Thorogood, 1984; Zhang et al., 2010). In the mature zebrafish fin, both skeletal structures occupy the epidermal-mesenchymal interface along the proximal-distal axis of the appendage, whereas the interior space of the fin is filled with vascularized and innervated mesenchymal tissue (Akimenko et al., 2003; Mari-Beffa and Murciano, 2010; Pfefferli and Jaźwińska, 2015). After adult fin amputation, the stump forms a new outgrowth, which is initially supported by actinotrichia before lepidotrichia formation (Duran et al., 2011; Mari-Beffa et al., 1989). Actinotrichia play at least two functions in the fin: providing mechanical support to the fin fold during swimming and acting as a substrate for the migration of mesenchymal cells during morphogenesis (Bhadra and Iovine, 2015; Duran et al., 2011; van den Boogaart et al., 2012; Wood and Thorogood, 1984; Zhang et al., 2010). The attachment of mesenchymal cells to the actinotrichial migratory substrate requires

* Corresponding author.
E-mail address: anna.jazwinska@unifr.ch (A. Jaźwińska).

http://dx.doi.org/10.1016/j.ydbio.2017.07.024
Received 19 May 2017; Received in revised form 25 July 2017; Accepted 27 July 2017
Available online 29 July 2017

Hemicentin 2 and Fibulin 1 matrix proteins (Feitosa et al., 2012).

Actinotrichia are composed of multiple collagenous and non-collagenous matrix proteins, which form a supramolecular aggregate, historically referred to as elastoidin (Galloway, 1985; Geraudie and Meunier, 1980; Mari-Beffa et al., 1989). By electron microscopy, actinotrichia exhibit a regular cross-banding, with a periodicity varying

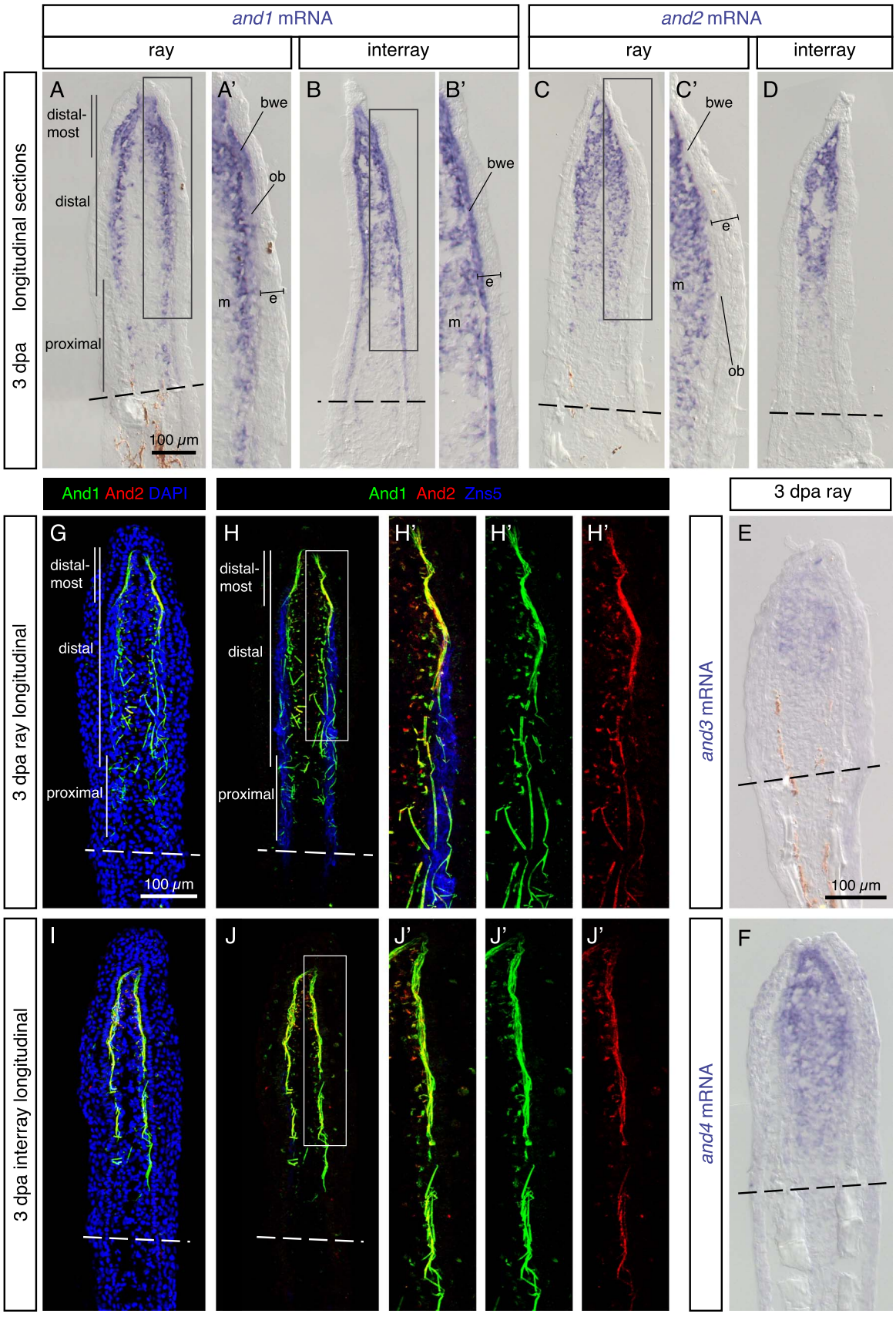

Fig. 1. Analysis of the actinotrichia-specific components in the regenerative outgrowth. (A-F) *In-situ* hybridization with probes against four *actinodin* genes on longitudinal fin sections at 3 dpa. N ≥ 4 fins; ≥ 3 sections per fin. (A, B) *and1* mRNA is detected in the mesenchyme (m) of the blastema and in the basal wound epithelium (bwe). No expression is detected in the basal wound epithelium adjacent to osteoblasts (ob) in the ray. (C, D) *and2* (E) *and3* (F) *and4* genes are co-expressed in the mesenchyme of the blastema, but not in the epidermis (e). (G-J) Immunofluorescence staining of longitudinal fin sections of ray (G, H) and interray (I, J) at 3 dpa. And1 (green) and And2 (red) proteins are co-localized in actinotrichia fibers. Rays and interrays are identified by the presence *versus* absence of Zns5-positive osteoblasts (H, J, blue). Actinotrichia fibers are predominantly found in the subepithelial position with the exception of osteoblast-containing regions. N = 4 fins; 3 sections per fin. Higher magnifications of framed areas are labeled with the same letter with a prime symbol. Fin amputation planes are shown with a dashed line. The same rules apply to all subsequent figures.

from 49 to 65 nm, depending on the species (Witten and Huysseune, 2007). Their unique architecture combines the rigidity of collagen fibers and the flexibility of elastic fibers, which might be advantageous for maintaining the structural integrity and the hydrodynamic function of the dermal fold (Galloway, 1985; van den Boogaart et al., 2012). Indeed, the biomechanical properties of actinotrichia are thought to be specific for swimming and irrelevant for walking on land, as the limb skeleton of terrestrial vertebrates lacks any actinotrichia-like structures (Lalonde et al., 2016; Sordino et al., 1995; Zhang et al., 2010). The unique components of these structures, called Actinodin (And) proteins, are fish-specific and were lost in the evolution of tetrapods (Zhang et al., 2010). Accordingly, Actinodin proteins are not involved in the support of the fin fold in aquatic tadpoles of amphibians.

In addition to the Actinodin proteins, fibrillar collagens, such as Collagen I and II, have been described to contribute to the composition of actinotrichia during development and regeneration (Bhadra and Iovine, 2015; Duran et al., 2015, 2011). In addition, a fibril-associated collagen, Collagen IX, has been shown to be required for actinotrichia integrity (Huang et al., 2009). Fish that carry a mutation in the *col9a1* gene, called *prp* mutants, develop shortened and deformed actinotrichia fibers. Based on the known function of Collagen IX in bridging Collagen type II fibrils (Huang et al., 2009), the *prp* phenotype suggests that supramolecular aggregation of fibrillar bundles is essential for shaping of actinotrichia.

Recent studies using transgenic reporter fish lines and functional assays have provided new insights into osteoblast de- and redifferentiation during lepidotrichia regeneration (Blum and Begemann, 2015; Brown et al., 2009; Knopf et al., 2011; Sousa et al., 2011; Stewart et al., 2014; Stewart and Stankunas, 2012; Thorimbert et al., 2015; Tu and Johnson, 2011; Wehner et al., 2014). Regeneration of actinotrichia has been studied using ultrastructural, immunohistochemical and gene expression approaches on fin sections (Duran et al., 2011; Govindan and Iovine, 2015; Mari-Beffa et al., 1989; Mari-Beffa and Murciano, 2010; Zhang et al., 2010). The regulation of actinotrichia formation in the regenerating fin has been addressed using chemical inhibition of Sonic Hedgehog signaling, Bone Morphogenetic Protein (BMP) receptors and Histone deacetylase 1 (Hdac1), which did not interfere with initial blastema formation, but led to a blockage of actinotrichia formation and progression of regeneration (Armstrong et al., 2017; Pfefferli et al., 2014; Quint et al., 2002; Thorimbert et al., 2015). However, the dynamic configuration of Actinodin-containing fibers during the entire fin restoration has not been investigated in detail. Moreover, the secretion of Actinodin proteins has not yet been assessed at the subcellular level. Finally, it remains unknown, whether the early blastema signals regulate actinotrichia formation and turnover during the outgrowth phase.

Here, we examined the temporal and spatial dynamics of actinotrichia regeneration by means of immunofluorescence analysis of Actinodin-1 in combination with lepidotrichial markers on whole-mount fins. We used *alf* mutants, which have longer and irregularly segmented lepidotrichia due to a potassium channel gain-of-function (Perathoner et al., 2014), to examine a correlation between enhanced fin growth and lengthened actinotrichia. We applied electron microscopy to detect fibrils assembling into thicker actinotrichia fibers specifically in the distal-most blastema, the site of their polymerization. Finally, we sought to characterize the importance of blastemal signaling pathways during actinotrichia regeneration, namely Fibroblast Growth Factor (FGF), Transforming Growth Factor β (TGFβ)/Activin-βA and Insulin-like Growth Factor (IGF). These analyses provide new insights into the dynamics of actinotrichia reestablishment during zebrafish fin regeneration.

2. Results

2.1. Two paralogous Actinodin proteins colocalize in the actinotrichia fibers of the regenerating fin

Four *actinodin* genes have been identified in the embryonic fin fold and were examined in adult fish (Nolte et al., 2015; Zhang et al., 2010). To compare the expression of all four *actinodin* transcripts in the regenerative outgrowth, we performed *in-situ* hybridization of longitudinal fin sections at 3 dpa, when actinotrichia massively emerge in the new tissue. Consistent with previous studies (Thorimbert et al., 2015; Zhang et al., 2010), *and1* was detected in the lateral mesenchyme of the blastema and in the basal layer of the wound epithelium (Fig. 1A, B). Interestingly, the *and1* probe labeled the basal wound epithelium more extensively in the interrays than in the rays. In the rays, the epithelial expression of this gene was restricted to the distal-most region, whereas it expanded further proximally in the interrays (Fig. 1A′, B′). By contrast, *and2/3/4* transcripts were detected in the distal blastemal mesenchyme, but not in the epidermis (Fig. 1C-F). The weakest staining was obtained for *and3,* which has not been detected by *in-situ* hybridization on whole-mount fins (Nolte et al., 2015). Thus, among all *actinodin* genes, only *and1* was present in the wound epithelium.

The localization of extracellular proteins cannot be solely inferred from the transcript distribution. Therefore, we raised antibodies against And1 and And2 unique peptides (less than 50% identity of amino acid sequences) in distinct species. First, we validated these antibodies on Western blot of fin regenerates at 3 dpa. And1 and And2 antibodies detected different proteins at relative molecular weight of approx. 75 kDa and 57 kDa, respectively (Fig. S1). Then, we used both antibodies for double immunofluorescence analysis of fin regenerates. The examination of longitudinal ray sections revealed that And1 and And2 co-localized in extracellular fibers in the regenerative outgrowth at 3 dpa (Fig. 1G-J). We concluded that both proteins jointly contribute to actinotrichia, despite the differences in gene expression patterns.

As previously reported (Duran et al., 2011; Thorimbert et al., 2015; Zhang et al., 2010), actinotrichia fibers were predominantly deposited along the lateral sides of the regenerative outgrowth between the wound epidermis and the blastema. This localization was particularly well established in the interrays (Fig. 1I, J). In the rays, which were recognized by the presence of Zns5-positive osteoblasts, actinotrichia fibers were longitudinally organized underneath the wound epithelium mainly in the distal-most part of the outgrowth (Fig. 1H′). In the distal and proximal part, which contained osteoblasts underneath the lateral epidermis, the And1-positive fibers were displaced into the mesenchymal compartment, which was often associated with a disruption of their longitudinal alignment.

In addition to the fibrillar pattern, both Actinodin antibodies recognized a dotty pattern laterally to the fibers, which might represent intermediate forms of actinotrichia fibers that undergo formation or turnover (Fig. 1H′, J′). We concluded that Actinodin 1 and Actinodin 2 proteins jointly contribute to the actinotrichia fibers in the regenerating zebrafish fin.

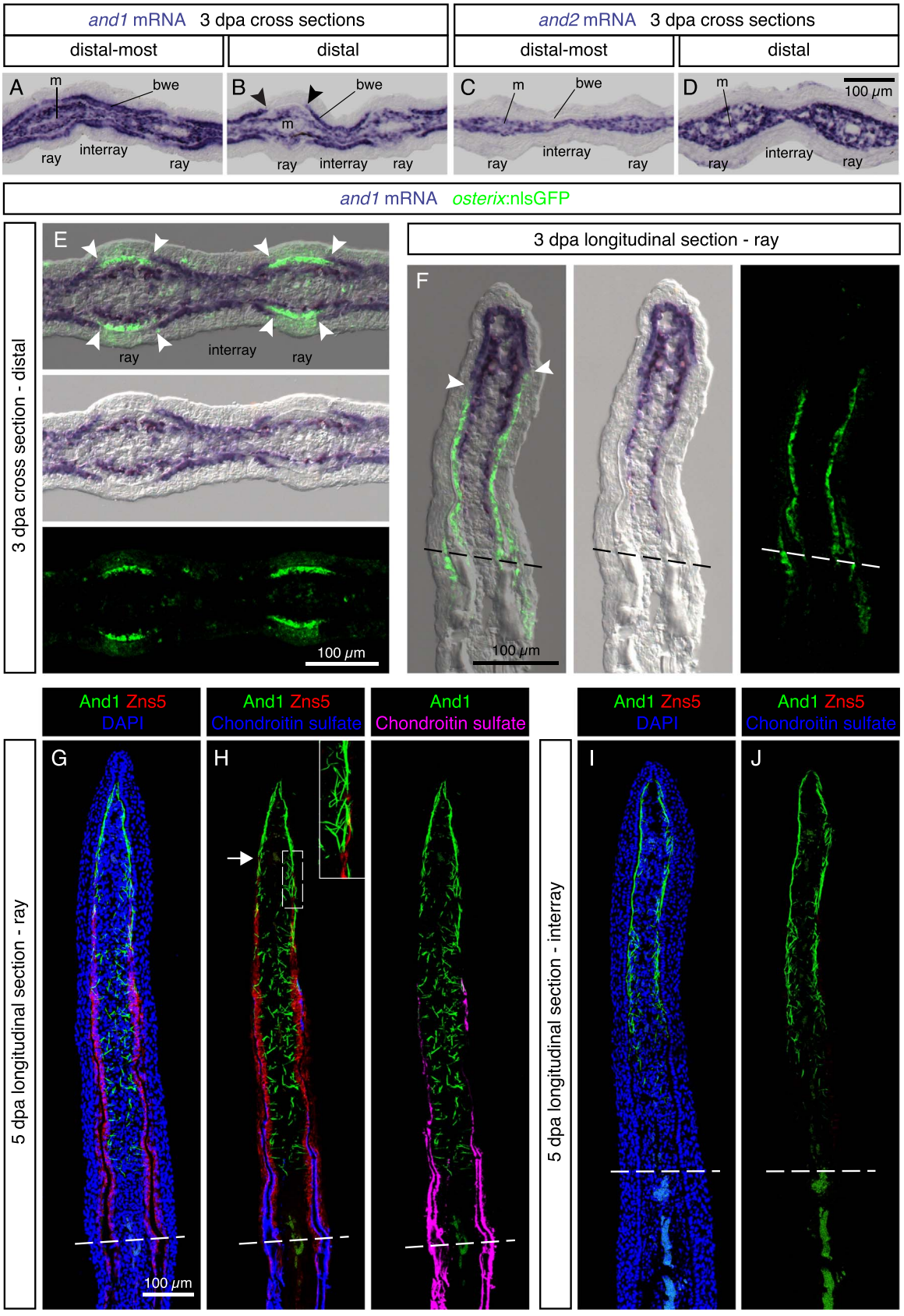
and1 mRNA 3 dpa cross sections
distal-most
distal
and2 mRNA 3 dpa cross sections
distal-most
distal
A
m
bwe
ray
interray
ray
B
bwe
m
ray
interray
ray
C
m
bwe
ray
interray
ray
D
m
100 μm
ray
interray
ray
and1 mRNA osterix:nlsGFP
3 dpa cross section - distal
E
ray
interray
ray
100 μm
3 dpa longitudinal section - ray
F
100 μm
And1 Zns5
DAPI
And1 Zns5
Chondroitin sulfate
And1
Chondroitin sulfate
And1 Zns5
DAPI
And1 Zns5
Chondroitin sulfate
5 dpa longitudinal section - ray
G
100 μm
H
5 dpa longitudinal section - interray
I
J

Fig. 2. Regenerating lepidotrichia replace actinotrichia in the subepidermal space. (A-D) *In-situ* hybridization on cross sections of distal-most and distal fin outgrowth at 3 dpa. N = 4 fins. (A, B) In the distal blastema, *and1* is differentially expressed in the basal wound epithelium of the rays and interrays. Arrowheads indicate the positions of the interrupted *and1* expression in the basal epithelium. m, mesenchyme; bwe, basal wound epithelium. (C, D) *and2* is absent from the wound epidermis. (E, F) *In-situ* hybridization against *and1* on transversal (E) and longitudinal sections (F) of *osterix:nlsGFP* transgenic fins. A lack of *and1* expression in the basal wound epithelium of rays is associated with the presence of underlying osteoblasts (green). Arrowheads indicate the positions of the interrupted *and1* expression in the basal epithelium. N = 6 fins, 2 sections per fin. (G-J) Immunofluorescence staining for And1 (green), Zns5 (red) and Chondroitin sulfate (H, J, blue) at 5 dpa. (G, H) In the ray, the leading edge of osteoblasts (arrow) replaces actinotrichia in the subepidermal compartment. In the mesenchyme, actinotrichia are disrupted and misaligned. (I, J) In the interrays, no Zns5 and chondroitin sulfate is detected. Actinotrichia remain longitudinally organized in the junctional region between the epidermis and the mesenchyme. The green signal at the base of the outgrowth corresponds to blood autofluorescence. N = 4 fins; 2 sections per fin.

2.2. Osteoblasts displace And1-positive fibers into the mesenchymal compartment

In-situ hybridization with the *and1* probe revealed a difference in the extent of the labeled basal wound epithelium between ray and interray (Fig. 1A, B). To further investigate this observation, we analyzed transversal sections of 3 dpa fin regenerates, in order to compare tissues of rays and interrays at the same proximo-distal level. As expected, *and2* mRNA was restricted to the mesenchyme (Fig. 2C, D), whereas *and1* expression in the basal wound epidermis was more complex (Fig. 2A, B). The sections through the distal-most regenerate displayed a continuous labeling with the *and1* probe in the basal wound epidermis of the rays and interrays (Fig. 2A), whereas in distal regenerate sections, a conspicuous gap in *and1* expression was detected in the wound epithelium of the rays (Fig. 2B). Thus, *in situ* hybridization on cross-sections clearly demonstrated that the epidermal expression of *and1* becomes downregulated in the distal and proximal part of the rays, without being changed in the adjacent interrays.

One of the structural differences between rays and interrays is the presence of the regenerating osteoblasts underneath the wound epidermis (Akimenko et al., 2003; Mari-Beffa and Murciano, 2010; Pfefferli and Jaźwińska, 2015). To determine the position of *and1* expressing cells in relation to osteoblasts, we performed *in situ* hybridization combined with a subsequent immunofluorescence staining on fin sections of *osterix(Sp7):nlsGFP* transgenic fish. Indeed, the absence of *and1* expression in the wound epithelium correlated with underlying GFP-positive osteoblasts, as examined on transversal and longitudinal sections (Fig. 2E, F). This finding suggests a possible negative regulation between osteoblasts and epithelial *and1* expression.

To determine whether the regenerating bones affect the organization of the And1-positive actinotrichia fibers at a more advanced regeneration stage, we examined fins at 5 dpa. At this stage, the proximal outgrowth undergoes differentiation, which coincided with a degradation of actinotrichia (Fig. 2G-J). To detect all osteoblasts, we applied the Zns5 antibody, whereas to detect bone matrix deposition, we visualized chondroitin sulfate (Montes et al., 1982). In the rays, the presence of the leading edge of Zns5-positive osteoblasts coincided with the displacement of actinotrichia from the subepithelial position into the mesenchymal compartment, even before chondroitin sulfate had been deposited (Fig. 2G, H). Thus, migrating osteoblasts and not deposited bone matrix seemed to be the primary structure associated with the perturbation of the alignment of actinotrichia fibers. Solely the distal-most tissue of rays displayed the organized and well-aligned actinotrichia underneath the wound epithelium. In the interrays, most of actinotrichia retained the longitudinal arrangement (Fig. 2I, J). These findings suggest that regenerating osteoblasts might interfere with the subepithelial organization of actinotrichia fibers, resulting in their misalignment. Thus, aligned actinotrichia fibers and lepidotrichia-forming cells are non-overlapping complementary skeletal elements of the regenerative outgrowth.

2.3. Actinotrichia formation in the distal-most outgrowth at the subcellular level

The distal-most part of the outgrowth does not comprise bone-forming cells, but it contains longitudinally organized actinotrichia. To characterize Actinodin-secreting cells, we performed high-resolution imaging of the epithelial-mesenchymal junctional region of the distal-most blastema on cross sections at 3 dpa (Fig. 3). In the transversal plane, Actinodin-labeled fibers appeared as circumferences of rods, indicating that the And1 and And2 antibodies detected predominantly the surface of actinotrichia (Fig. 3A-B). The visualization of the cytoplasm using α-Tubulin immunostaining showed that mesenchymal cells appeared to partially engulf the adjacent actinotrichia fibers (Fig. 3B′, B″). Thus, blastema cells display a marked physical contact to Actinodin-coated actinotrichia, consistent with a function of these fibers as a substrate for guided cell migration during regeneration (Wood and Thorogood, 1984, 1987).

Next, we focused on intracellular distribution of Actinodin proteins. Both And1 and And2 were detected in the cytoplasm in a dotted pattern, suggesting a vesicular transport in the secretory pathway (Fig. 3C-E). In the blastemal mesenchyme, And1 and And2 formed together a granular aggregate in the peri-nuclear region of mesenchymal cells. These aggregates colocalized with a *cis*-Golgi marker, GM130 (Fig. 3F). Consistent with the *in-situ* hybridization analysis, only And1, but not And2, was detected in the cells of the basal layer of the wound epidermis (Fig. 3C, D). These data provide evidence that in the distal-most outgrowth, epidermal cells secrete And1, whereas mesenchymal cells produce both And1 and And2.

The ultrastructure and properties of elastoidin, the actinotrichial substance, have previously been characterized by electron microscopy, X-ray diffraction studies and biophysical and chemical analysis (Galloway, 1985). In zebrafish, *de-novo* formation of actinotrichia fibers during regeneration has not yet clearly been demonstrated. To observe the fibrogenesis of actinotrichia, we performed electron microscopy analysis specifically of the distal-most outgrowth at 3 dpa. To detect And1, we first applied immunohistochemical antibody staining using the DAB-Peroxidase reaction on longitudinal sections. As DAB is electron dense, the DAB-labeled tissue is expected to be darker than in control samples, which were treated with the same protocol but without the primary And1 antibody. As previously reported (Becerra et al., 1996; Bechara et al., 2003; Huang et al., 2009; Mari-Beffa et al., 1989; van den Boogaart et al., 2012; Wood and Thorogood, 1987), the electron microscopy images of actinotrichia displayed collagen-like striated fibers with the main periodic striation of approx. 60 nm (Fig. S2A, A′). The samples that were exposed to the And1 antibody appeared darker than control samples, validating the antibody immunoreactivity in these structures (Fig. S2B). We found that the extracellular matrix of the distal-most blastema contained abundant 20 nm fibrils that were arranged nearly parallel to each other (Fig. S2A, A″). Notably, these fibrils appeared to aggregate through parallel contacts into thicker higher-order fibers, suggesting actinotrichia polymerization in width and in length (Fig. S2A″, B′). These data suggest that actinotrichia assemble from preformed intermediates, a process reminiscent of collagen fibrogenesis, which is consistent with ultrastructure analysis during zebrafish development (Birk and Brückner, 2011; Dane and Tucker, 1985). From the structural viewpoint, it is remarkable that despite the presence of non-collagenous components, such as Actinodin proteins, the fibers display clean cross-striations in a collagen-like configuration.

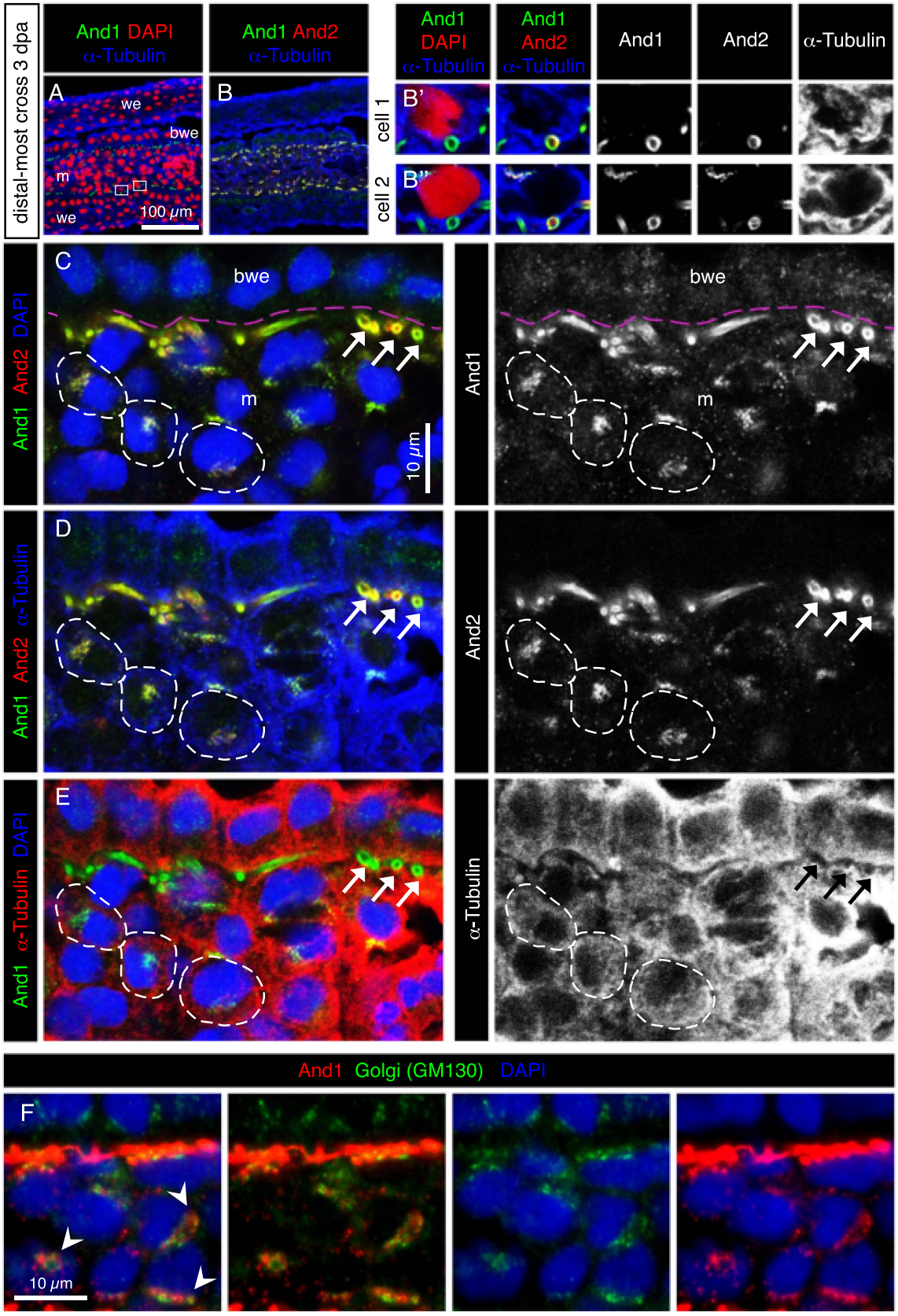

Fig. 3. The subcellular distribution of And1 and And2 suggests their vesicular transport in mesenchymal cells. (A-F) Immunofluorescence staining of transversal sections of the distal-most outgrowth at 3 dpa (A-E) Quadruple staining for And1, And2, the cytoplasmic marker α-Tubulin and nuclear DAPI. (A, B) Overview of the tissue and magnification of two cells in the blastema. And1/2 antibodies detect ring-like structures, which are cross-sections of actinotrichia fibers. Actinotrichia are partially engulfed by mesenchymal cells, but remain extracellular. (C-E) The same specimen of the distal-most outgrowth presented in a different combination of stainings and colors. Pink dashed lines indicate the position of the basement membrane. And1 and And2 colocalize at the circumference of actinotrichia fibers (white arrows). Dotted distribution of both proteins in the α-Tubulin-labeled cytoplasm (dashed outline) indicates a subcellular localization in the vesicular system. And1 is detected in the basal wound epithelium and mesenchyme, while And2 is detected only in the mesenchyme. N = 4 fins. (F) Immunofluorescence for Golgi matrix protein GM130 (green) and And1 (red), showing colocalization of both markers in a form of perinuclear aggregates. m: mesenchyme, we: wound epidermis, bwe: basal wound epithelium. N = 4 fins.

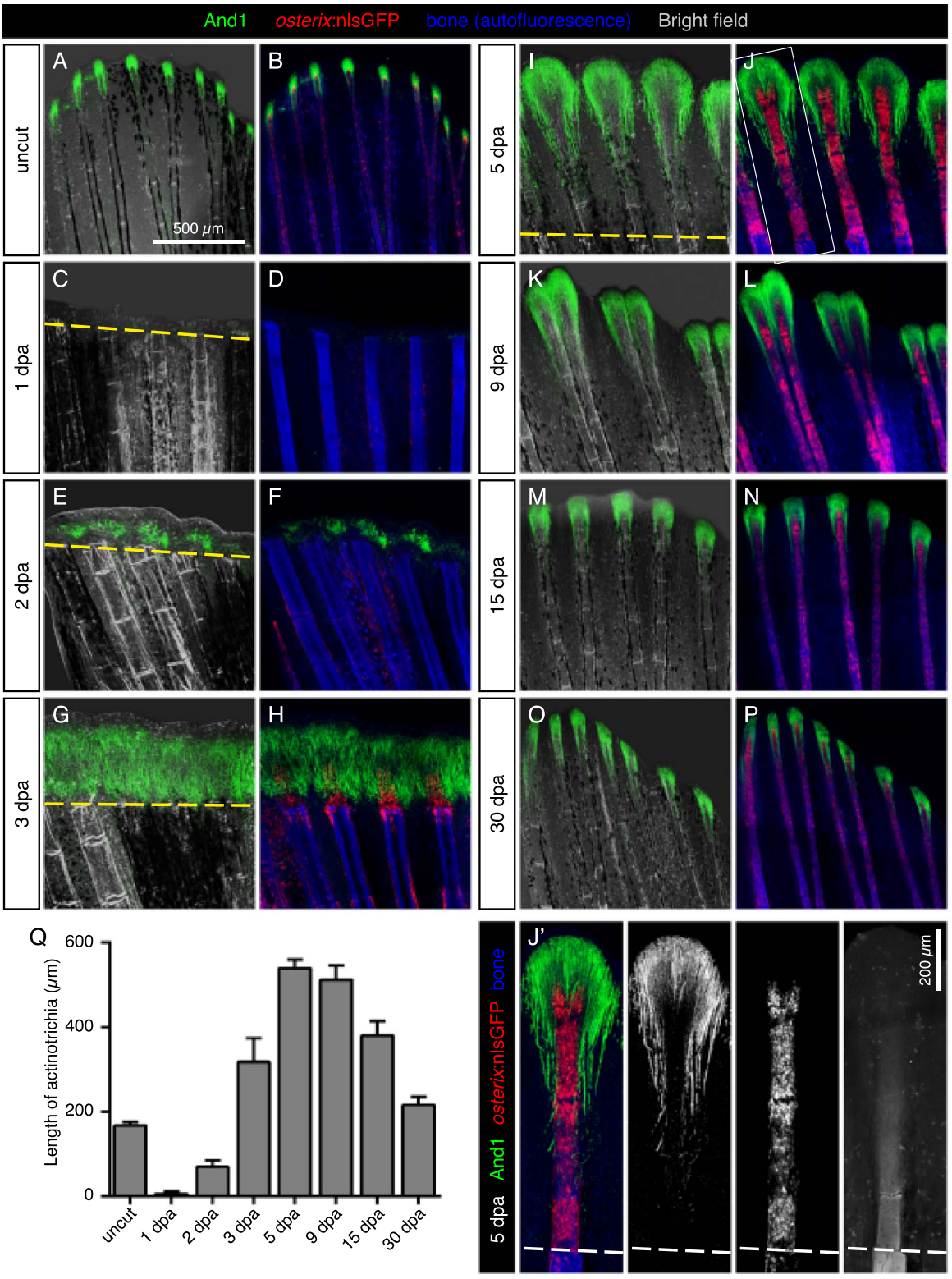

Fig. 4. Dynamics of actinotrichia regeneration correlate with lepidotrichia regrowth. (A-P) Immunofluorescence staining for And1 (green) in *osterix:nlsGFP* fish (osteoblasts; red) at different time points after amputation (dpa). Bone matrix/tissue autofluorescence shown in blue. (Q) Quantification of the length of And1-positive regions at different time points during regeneration. Each fin was represented by the measurements of the second, third, and fourth ray relative to the edge of both lobes. N ≥ 4 fins for each time point. 6 rays per fin. Error bars represent SEM. (J′) Magnification of a single ray at 5 dpa, showing inverse correlation between And1 deposition and *osterix:nlsGFP*. The V-shaped tip of the regenerating lepidotrichium indicates an initiated ray bifurcation.

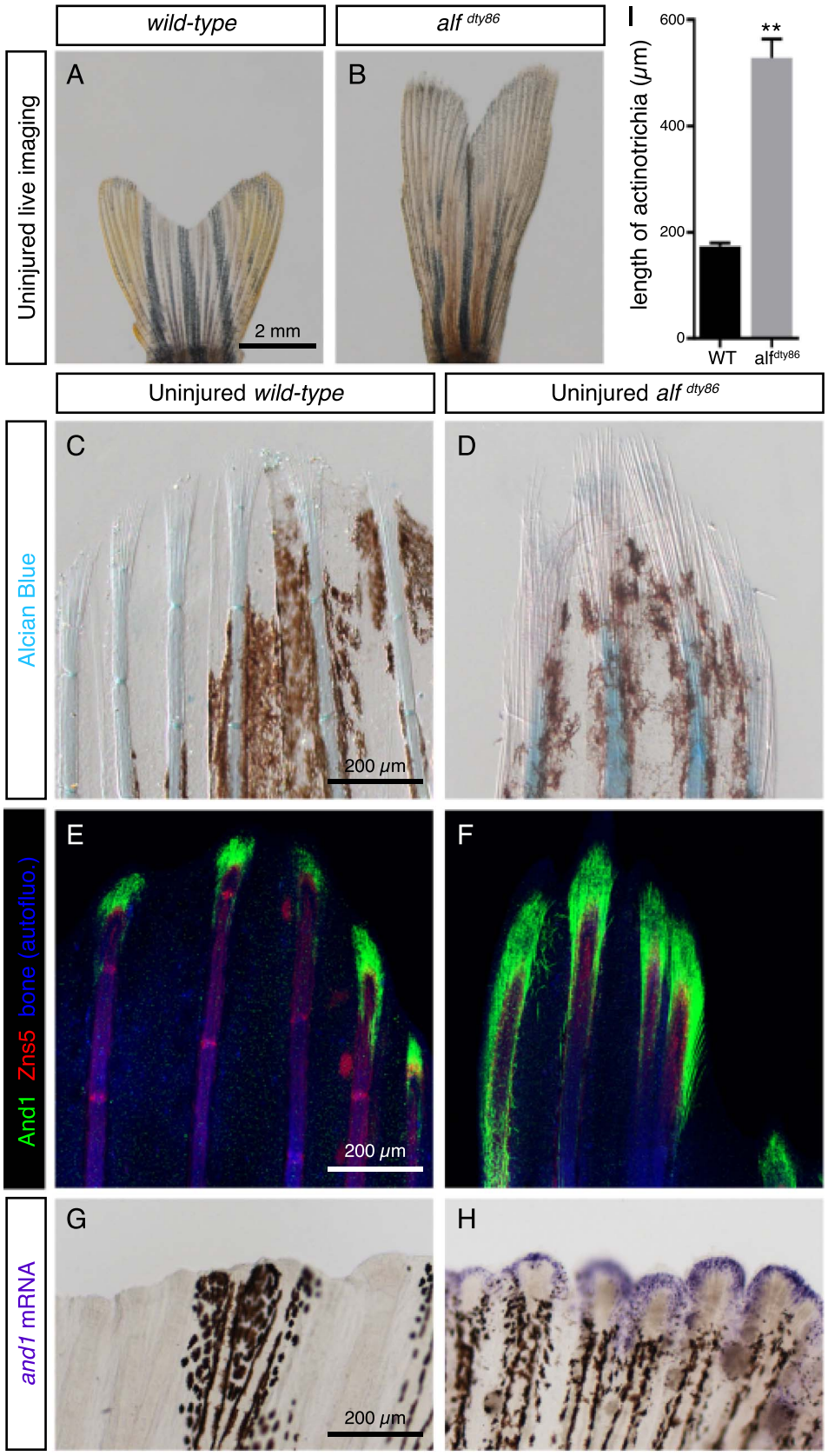

Fig. 5. Elongated uninjured fins of *alf* ^{dty86} mutant fish contain extended actinotrichia. (A, B) Live-imaging of adult caudal fins in wild-type fish and *alf* ^{dty86} mutants. (C, D) Alcian blue histological staining of uninjured caudal fins shows uncalcified lepidotrichia/cartilage (blue). Bundles of actinotrichia are unstained, but visible by a differential contrast at the tips of rays. Brown patches correspond to endogenous fin pigmentation. N = 4 fins. (E, F) Double immunostaining of wild-type and *alf* ^{dty86} mutant fins using And1 (green) and osteoblast marker Zns5 (red) antibodies. Tissue autofluorescence shown in blue. N = 4 fins. (G, H) *In-situ* hybridization with *and1* probe on whole-mount fins labels uninjured fin margin of *alf* ^{dty86} mutant fins, but not wild-type ones. N = 5 fins. (I) Quantification of length of actinotrichia in wild-type *versus alf* ^{dty86} uninjured fins based on And1 staining (6 rays quantified for each fin, N = 4 fish per group. Error bars indicate SEM, ** $P < 0.01$).

2.4. Dynamics of actinotrichia size throughout the regenerative process

Appendage regeneration involves re-establishment of the distal identity after amputation. As actinotrichia are considered the distal skeletal elements of the fin, we set out to determine the dynamics of actinotrichia reestablishment during the progressive reconstitution of the missing appendage parts. Specifically, we aimed to monitor the length of the actinotrichial tissue and its position relative to regenerating lepidotrichia at different time points of regeneration. Therefore we performed And1 immunofluorescence analysis on whole-mount fins of *osterix(Sp7):nlsGFP* fish, which demarcate committed osteoblasts, at different time points (Fig. 4). After imaging, we performed histological Alizarin red/Alcian blue staining of the same fins to detect the level of bone matrix deposition and mineralization (Fig. S3). And1 immunofluorescence detected actinotrichia in uninjured fins at the ray tips (Fig. 4A, B). During the onset of blastema formation at 1 dpa, the stump did not show And1 expression, indicating that the activated pre-existing tissue is not capable of *de-novo* actinotrichia formation (Fig. 4C, D). However, already at 2 dpa, when the blastema starts to protrude beyond the amputation plane, And1-positive actinotrichia fibers emerged in the new tissue (Fig. 4E, F). At 3 dpa, actinotrichia massively populated the entire regenerative outgrowth (Fig. 4G, H). Thus, as previously reported (Duran et al., 2011; Zhang et al., 2010), during the early regenerate formation stage, actinotrichia are densely synthesized exclusively in the newly formed tissue that protrudes beyond the injury plane. The absence of actinotrichia in the stump suggests that the ability of switching from the original proximal to the distal skeletal identity is restricted to the newly generated tissue.

During the advanced regenerative outgrowth stage, the blastema cells undergo progressive differentiation in the proximo-distal direction (Pfefferli and Jaźwińska, 2015; Tornini and Poss, 2014; Wehner and Weidinger, 2015). At 5, 9 and 15 dpa, the highest accumulation of And1-positive actinotrichia was consistently observed at the apical part of the regenerate, while the lowest amounts of these structures remained at the proximal position of the outgrowth (Fig. 4I-N). This observation suggests that And1-immunoreactive fibers are maintained in undifferentiated tissue of the fin regenerate. In the rays, the proximal part of actinotrichia fibers, which can be observed by histological staining of the same specimens (Fig. S3), did not display And1-immunoreactivity, due to the limited penetrance of antibodies through the bone layers. After the fin re-growth reached termination, at 30 dpa, And1-labeled actinotrichia nearly recapitulated the pattern and size observed in uninjured fins (Fig. 4O, P). In the rays, these fibers inversely correlated with the regenerating osteoblasts (Fig. 4J′). To quantify the And1-positive actinotrichia, we measured the length of the And1-positive fibers laterally to bones in the interray. Remarkably, the length of the And1 positive tissue was dynamic throughout regeneration, reaching the maximal length of 550 µm at 5 dpa, and progressively diminishing at subsequent time points until the original size was

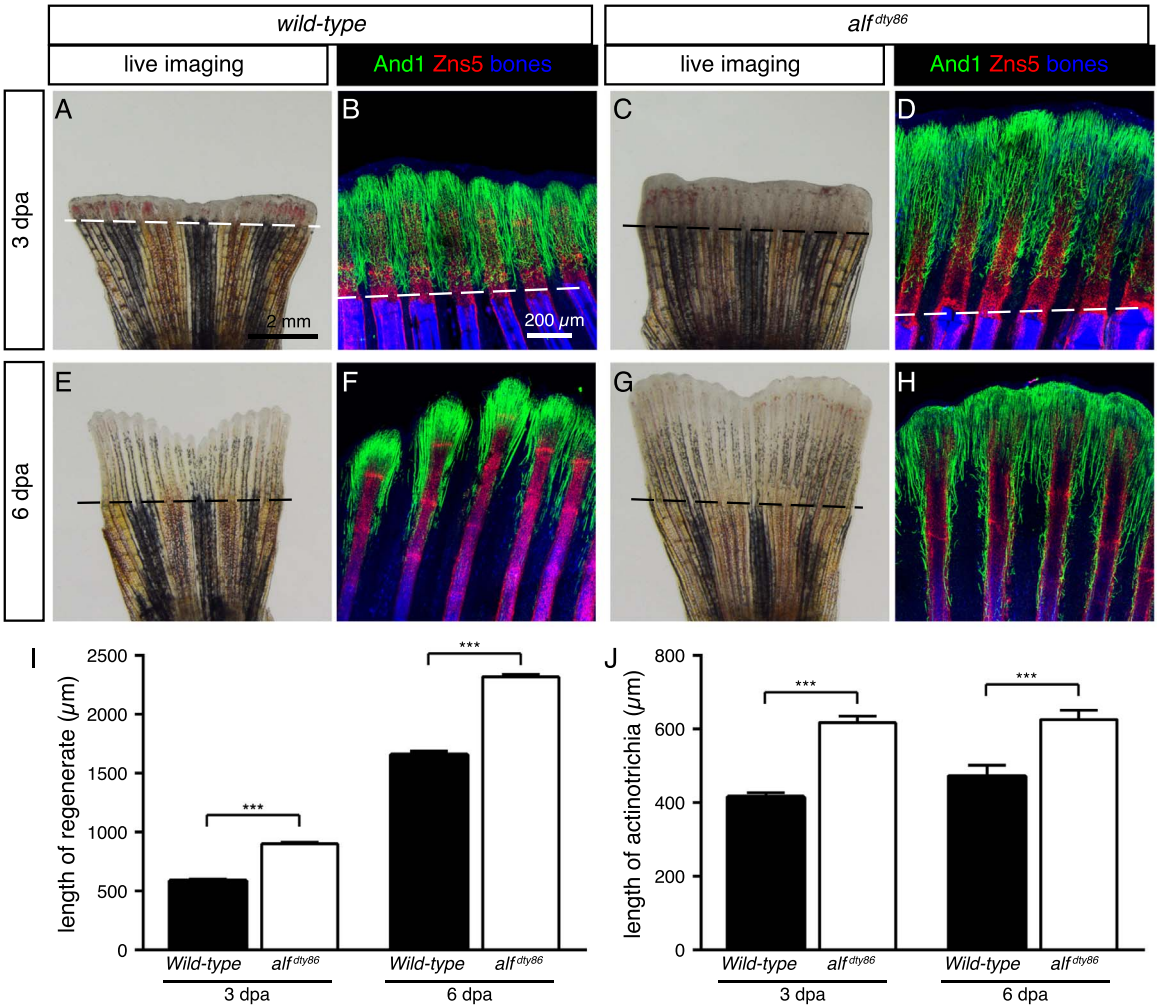

Fig. 6. Accelerated fin regeneration in *alf* ^{dty86} mutant fish is accompanied by elongated actinotrichia. (A, C, E, G) Live-imaging of wild-type and *alf* ^{dty86} mutant fins at 3 and 6 dpa. The regenerative outgrowth is more advanced in *alf* ^{dty86} mutant fins as compared to control. (B, D, F, H) Whole-mount immunofluorescence staining against And1 (green) and Zns5 (red). Bone/tissue autofluorescence shown in blue. And1-positive tissue is elongated in the regenerative outgrowth of *alf* ^{dty86} mutant fins. N ≥ 4 fish per group. (I, J) Quantification of the outgrowth and actinotrichia length at 3 and 6 dpa. (N ≥ 4 fins for each time point. 6 rays per fin. Error bar indicates SEM, *** P < 0.001).

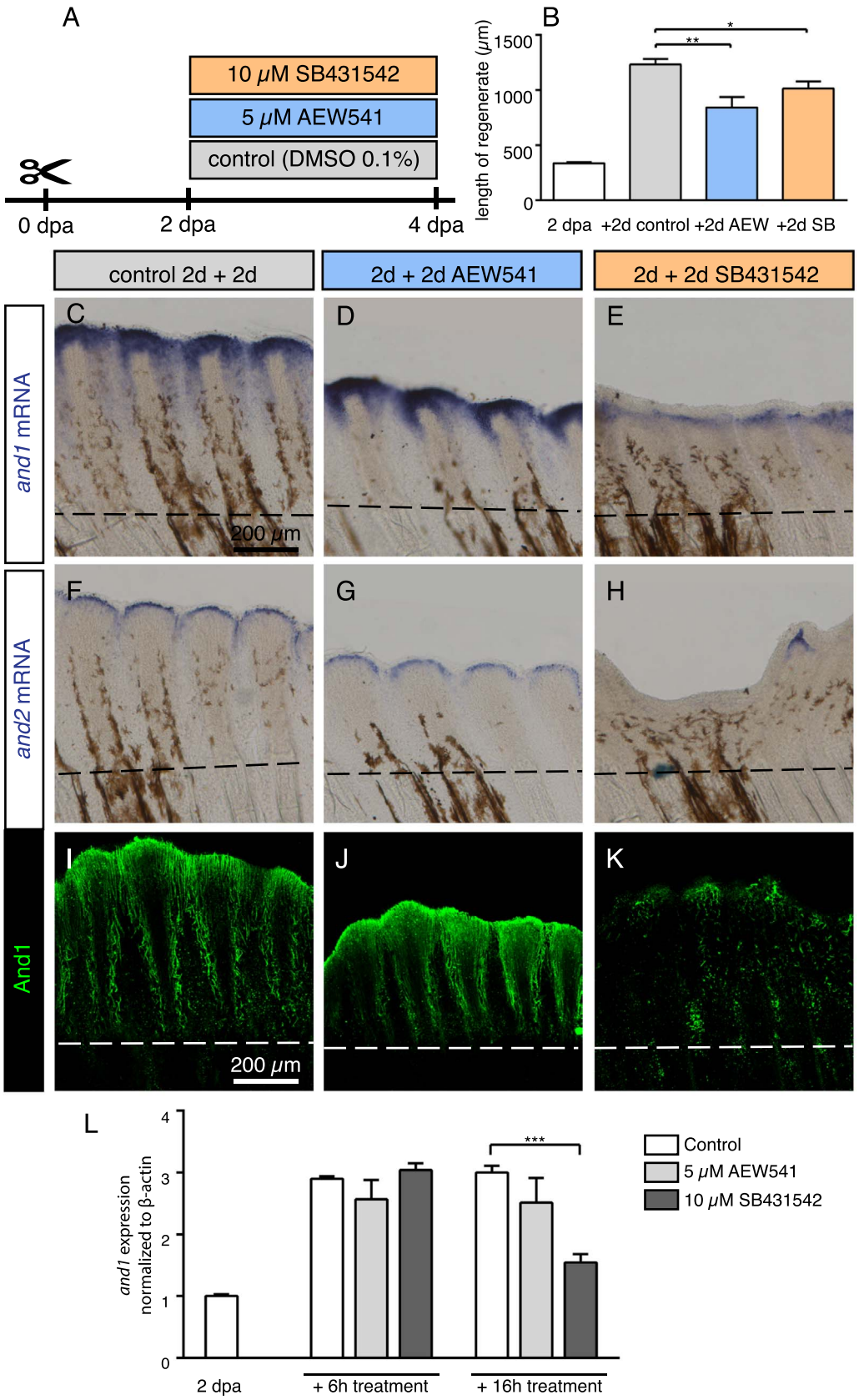

Fig. 7. Modulation of *and1* and *and2* expression in response to pulse inhibition of TGFβ/Activin-βA and IGF signaling. (A) Experimental design for inhibition of TGFβ/Activin-βA signaling by SB431542 and of IGF signaling by AEW541. (B) Quantification of length of regenerate as the average length of the second, third, and fourth rays from the lateral edge of the fin. N ≥ 4 for each group. Error bar indicates SEM, *P < 0.05, ** P < 0.01. (C-H) Whole-mount *in-situ* hybridization for *and1* and *and2* on 4 dpa fins. Inhibition of TGFβ/Activin-βA (SB431542) blocked expression of both genes, whereas inhibition of IGF (AEW541) had no effect. (I-K) Whole-mount immunofluorescence staining for And1 (green) on 4 dpa fins. TGFβ/Activin-βA inhibition (K) caused a loss of actinotrichia as compared to control (I) and IGF inhibition (J). (L) qRT-PCR analysis of *and1* expression after 6 h or 16 h of treatment with the pharmacological inhibitors AEW541 (IGF pathway) and SB431542 (TGFβ/Activin-βA pathway). Treatments started at 2 dpa. The relative expression was normalized to control fins at 2 dpa. N = 3 (9 fins each). Error bars represent SEM, *** P < 0.001.

reached (Fig. 4Q). This observation supports the notion that during the entire regenerative process, actinotrichia undergo a dynamic turnover and are confined to the distal fin skeleton (Bhadra and Iovine, 2015; Mari-Beffa et al., 1989).

To further visualize the arrangement of actinotrichia fibers in the outgrowth, we performed a 3-D reconstruction of the And1 immunofluorescence staining in whole mount fins. The analysis of projections revealed a bilateral distribution of parallel fibers along the proximo-distal axis in uninjured and 3 dpa fins (Fig. S4 and Movie 1 and 2). A dense network of And1-positive actinotrichia underneath the lateral epidermal surfaces appeared to encase the medially located mesenchyme.

2.5. *alf* mutant fins develop abnormally elongated actinotrichia during homeostasis and regeneration

Our analysis revealed that the distribution of And1-positive actinotrichia and lepidotrichia were complementary during regeneration. To further determine whether the size determination of lepidotrichial segments and actinotrichia fibers are co-regulated in the fin, we analyzed *another longfin* (*alf* ^{dty86}) mutant fish, which carry a gain-of-function mutation in *kcnk5b*, a gene encoding a potassium channel (Perathoner et al., 2014; van Eeden et al., 1996). This mutation causes elongated fins in proportion to the body size, due to the enlarged and irregular length of lepidotrichial segments (Fig. 5A, B) (Perathoner et al., 2014). It has been also reported that the organization and diameter of actinotrichia are partially affected in the fin regenerate of *alf* ^{dty86} (Bhadra and Iovine, 2015). Here, we examined whole-mount fins to determine the length of actinotrichia. To visualize actinotrichia in uninjured fins, we performed Alcian blue histological staining and immunofluorescence analysis with And1 and Zns5 antibodies. Interestingly, we found that uninjured *alf* ^{dty86} fins contained approximately 3-times longer actinotrichia in comparison to wild type fins (527 μm ± 36 *vs.* 172 μm ± 7) (Fig. 5C-F, I). Moreover, whole-mount *in-situ* hybridization detected enhanced expression of *and1* along the fin margin of *alf* ^{dty86} mutant fish, suggesting an enhanced synthesis of actinotrichia during homeostasis (Fig. 5G, H). These data indicate that the activity of potassium channels directly or indirectly regulates the length determination of both skeletal structures, not only lepidotrichial segments, but also actinotrichia.

Previous studies demonstrated that *alf* ^{dty86} mutant fish display accelerated regeneration due to elevated cell proliferation (Govindan and Iovine, 2014; Perathoner et al., 2014). To determine whether this phenotype is associated with changes in the actinotrichia length, we analyzed *alf* ^{dty86} mutant fins at 3 and 6 dpa (Fig. 6A-H). Double staining of whole mount fins with And1 and Zns5 antibodies revealed that at both time points, the regenerative outgrowth and the And1-labeled fibers were significantly extended in comparison to wild type regenerates (Fig. 6I, J). Thus, the phenotype of *alf* ^{dty86} mutants is associated not only with the overgrowth of lepidotrichial segments, but also with the prominent elongation of actinotrichia fibers during both homeostasis and regeneration.

2.6. Actinotrichia formation is regulated by TGFβ/Activin-βA and FGF signaling during fin regeneration

The description of molecular mechanisms regulating actinotrichia regeneration is still incomplete. We used a candidate approach to examine the impact of several signaling pathways on actinotrichia during fin regeneration. To investigate whether the IGF and the TGFβ/Activin-βA signaling pathway are required for actinotrichia regeneration, we applied previously characterized pharmacological inhibitors NVP-AEW541 and SB431542, respectively, which block blastema formation (Chablais and Jazwinska, 2010; Jazwinska et al., 2007). In the absence of the blastema, actinotrichia formation was not detected (data not shown). Therefore, we designed a drug-shift experiment, in which the treatment with inhibitors was performed for 2 days starting at 2 dpa, after the initial formation of the blastema (Fig. 7A). Consistently with previous studies, the exposure to NVP-AEW541 or SB431542 resulted in a shorter outgrowth as compared to control, indicating the impaired progression of regeneration (Fig. 7B). However, only the inhibition of TGFβ/Activin-βA signaling, but not IGF signaling, reduced *and1* and *and2* mRNA expression and And1 immunoreactivity in the impaired outgrowth (Fig. 7C-K). In order to determine how fast TGFβ/Activin-βA inhibition affects *and1* expression, qRT-PCR analysis was conducted on fin regenerates after 6 and 16 h of drug treatment. After 6 h exposure to NVP-AEW541 or SB431542, we did not observe any difference in the expression of *and1*, suggesting that TGFβ/Activin-βA may not directly regulate actinotrichia formation (Fig. 7L). By contrast, 16 h exposure to SB431542, but not NVP-AEW541 reduced *and1* expression (Fig. 7L). These results suggest that actinotrichia formation and maintenance are regulated by the TGFβ/Activin-βA signaling pathway, however, probably in an indirect manner. Moreover, a prolonged exposure during 14 days of uninjured fins to SB431542 did not affect the pre-existing actinotrichia (data not shown). Thus, TGFβ/Activin-βA signaling is not essential for the maintenance of actinotrichia during homeostasis, but only during regeneration.

The FGF signaling pathway has been known for a long time as a major regulator of zebrafish regeneration (Lee et al., 2005; Poss et al., 2000; Whitehead et al., 2005). To investigate the role of the FGF pathway in actinotrichia regeneration, we used the transgenic fish *hsp70:dnfgfr1-egfp*, which overexpress a dominant negative form of the FGF receptor type 1 after heat shock induction (Lee et al., 2005). The heat shock was induced at 2 dpa, after the establishment of the normal blastema and the beginning of actinotrichia formation. The examination of fins on the subsequent day, at 3 dpa, showed a reduced expression of *and1* mRNA and severe suppression of the And1 deposition (Fig. 8A, B, D, E, G, H). A similar phenotype was observed after a pharmacological inhibition of the FGF signaling pathway using 10 μM PD173074. After one day of treatment, at 3 dpa, the blastema retained only rudimentary And1-positive actinotrichia in the impaired regenerate (Fig. 8J, K). A drastic reduction of *and1* expression was also observed in qRT-PCR analysis after 6 h of treatment with PD173074, indicating that FGF pathway might directly regulate actinotrichia (Fig. 8L). The decrease in And1-labeled fibers after transgenic and pharmacological inhibition indicates that FGF signaling is not only necessary for *de novo* formation of actinotrichia, but also for the maintenance of pre-existing fibers.

To further determine the role of FGF in actinotrichia regeneration, we applied a genetic approach by using *fgf20a* homozygous mutant fish called *devoid of blastema* (*dob*), which fail to regenerate fins (Whitehead et al., 2005). At 3 dpa, we identified a few *dob* mutant fins that displayed rudimentary outgrowths. Nevertheless, the wound epidermis and mesenchyme of the protruding tissue lacked *and1* expression above the amputation plane (Fig. 8C, F, I). The examination of uninjured fins in this mutant revealed normal actinotrichia length and morphology (data not shown). Thus, *fgf20a* is not required for actinotrichia formation during normal fin growth, but it is essential for *and1* gene expression after amputation. Taken together, the transgenic, pharmacological and genetic assays consistently demonstrate the essential role of FGF signaling for actinotrichia regeneration.

Finally, we investigated the ability of fins to resume actinotrichia regeneration after transient inhibition. For the pharmacological experiments, the fish were exposed to the inhibitors of TGFβ/Activin-βA, IGF and FGF signaling for 2 days starting at 2 dpa, followed by another 6 days of recovery in normal conditions (Fig. S5A-C). For the transgenic overexpression of the dominant negative FGF receptor, *hsp70:dnfgfr1-egfp* fish were exposed to a heat shock at 2 dpa and subsequently left to regenerate without any further disturbance until 10 dpa (Fig. S5D-F). In all cases, actinotrichia resumed regeneration during the recovery period, and were similar to those of control fins at

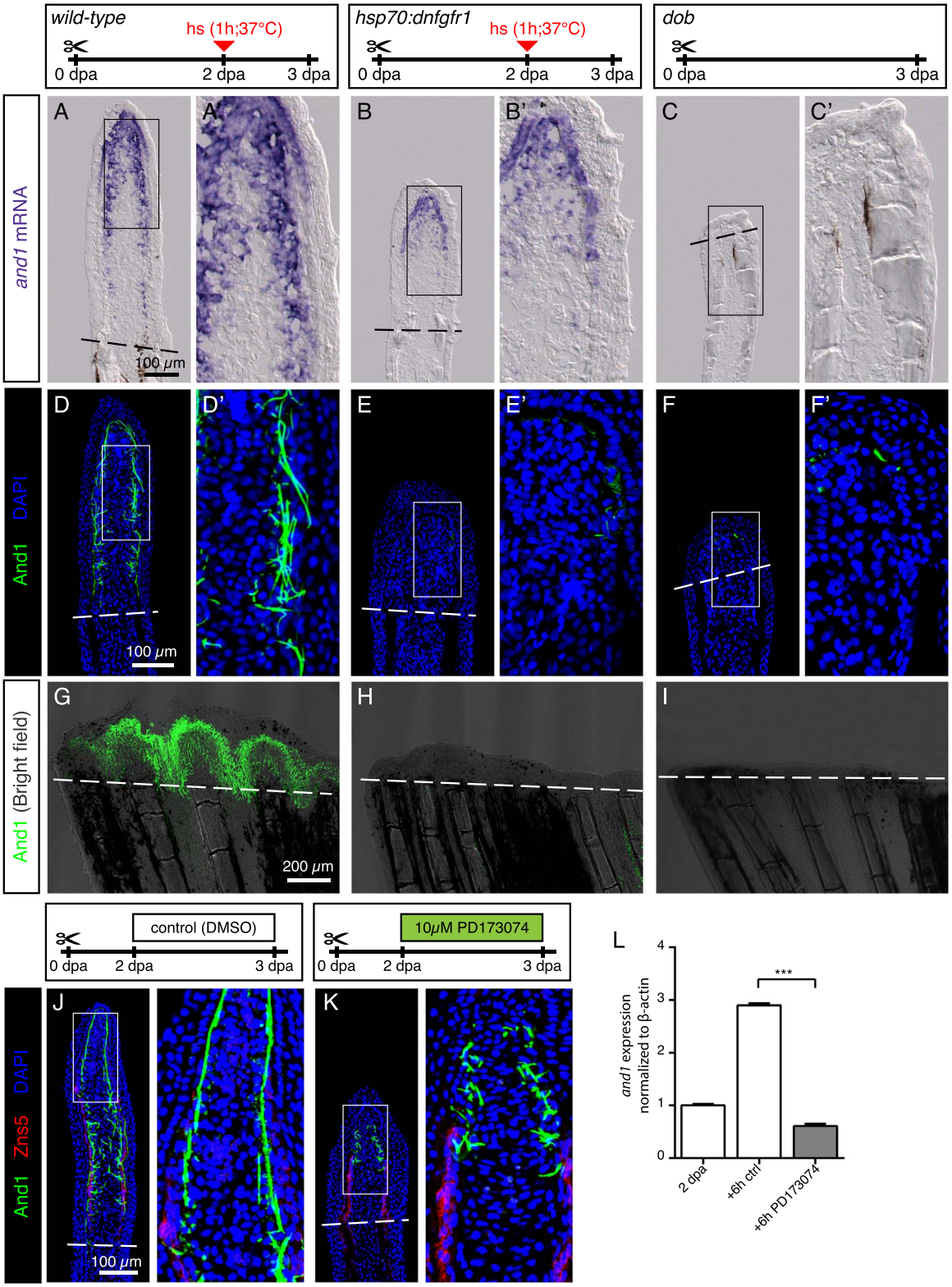

Fig. 8. FGF signaling is essential for actinotrichia formation and maintenance. (A-C) *In-situ* hybridization for *and1* on 3 dpa sections in control, *hsp70:dnfgfr1-egfp* and *dob* fish. Control and *dnfgfr1* fish underwent heat shock (hs) at 2 dpa. N = 4 fins per group. (D-F) Immunofluorescence for And1 (green) on longitudinal sections at 3 dpa in control, *hsp70:dnfgfr1-egfp*, and *dob* fish. N = 4 fins per group. (G-I) Whole-mount immunofluorescence staining for And1 (green) overlaid with bright field images for all experimental groups. N = 3 fins per group. Both, transgenic expression of *dnfgfr1* and *dob* mutation cause a drastic decrease in *and1* expression (B-C) and And1 deposition (E-F, H-I). (J, K) Immunofluorescence staining with And1 (green) and Zns5 (red) on 3 dpa longitudinal sections of fins of control fish and fish treated with PD173074 for 1 day. One day of treatment with the inhibitor of FGF signaling starting at 2 dpa is sufficient to disrupt actinotrichia in the blastema. N = 4 fins. (L) qRT-PCR analysis of *and1* expression after 6 h of treatment with 10 µM of the pharmacological inhibitor of the FGF pathway, PD173074. Treatment started at 2 dpa. The relative expression was normalized to control fins at 2 dpa. N = 3 (9 fins each). Error bars represent SEM. *** $P < 0.001$.

10 dpa. We concluded that actinotrichia can be reestablished after their degradation due to transient inhibition of inductive pathways.

3. Discussion

Actinotrichia are fin-specific skeletal structures that arise by aggregation of collagens with other associated proteins. The unique components of these elements are Actinodin proteins, which have not been shown in any other tissue and are not conserved in tetrapods (Lalonde et al., 2016; Zhang et al., 2010). Thus, Actinodin proteins may determine the distinctive biophysical properties of actinotrichia, which are specialized for supporting the flattened extremity during swimming (van den Boogaart et al., 2012). Using specific antibodies, we demonstrated that two paralogous Actinodin proteins, epithelial-mesenchymal And1 and mesenchymal And2, jointly contribute to actinotrichia fibers. We identified that beside the well-aligned arrays of actinotrichia in the subepidermal space in the distal-most ray blastema, the distal and proximal ray blastema also contains And1-labeled actinotrichia, however, in a more disorganized configuration underneath the regenerating osteoblasts (Fig. 9). Interestingly, only the surface of the fibrils was immunoreactive for And1/2 antibodies. This localization suggests that actinodins are deposited on the surface of the rods, where they could play an essential role for linking mesenchymal cells to actinotrichia. On the other hand, however, it is possible that the dense molecular packing within the fibrillar core hinders the accessibility of the epitopes for immunodetection (Galloway, 1985; Hulmes et al., 1995). In addition to the extracellular localization of Actinodin, we detected these proteins in the intracellular secretory pathway. Further studies will be essential to understand the mechanisms regulating assembly of actinodins with collagens and their interaction with cell surfaces.

Previous studies of fins in various fish species suggested that structural interactions may occur between actinotrichia and lepido-

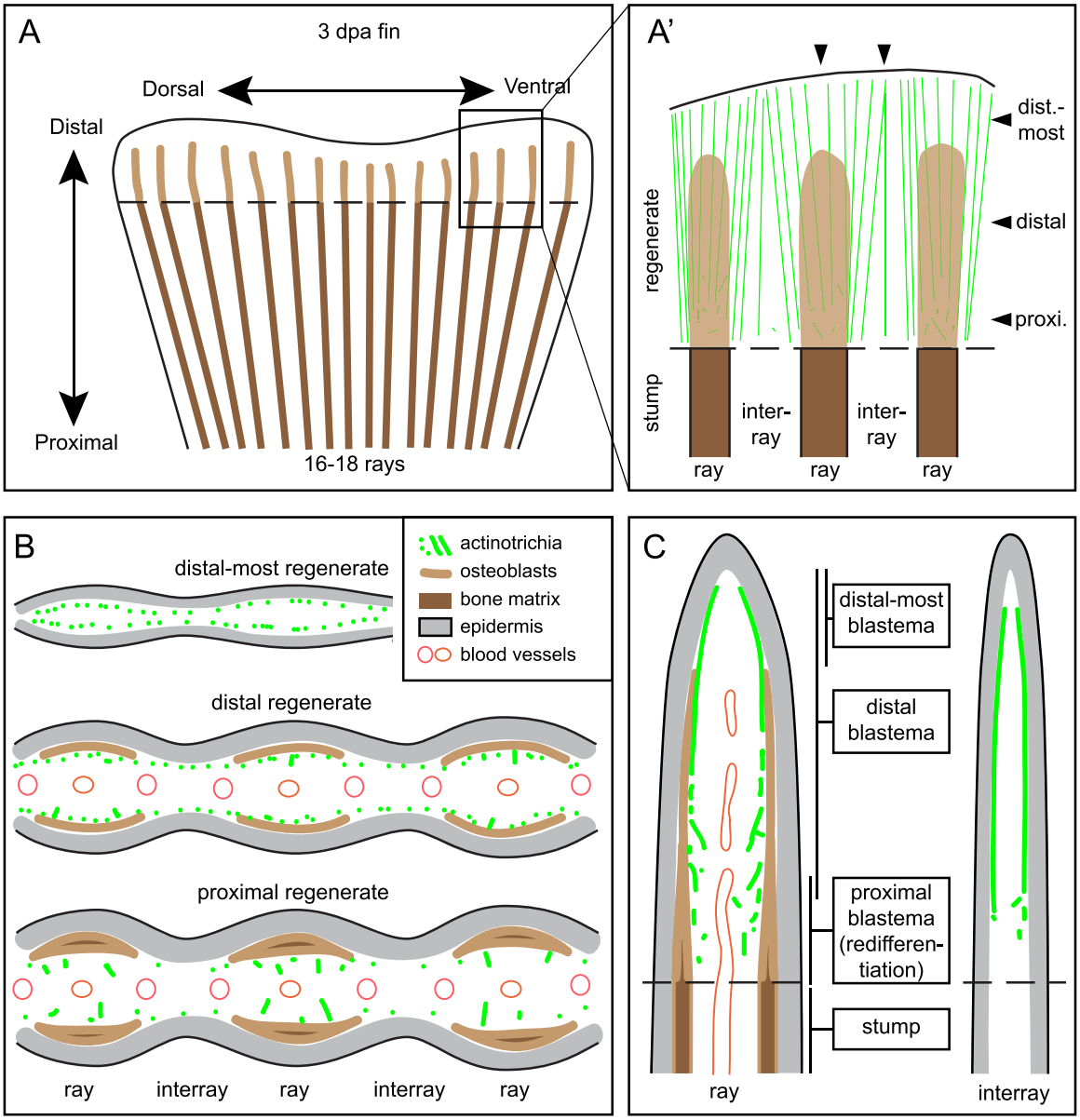

Fig. 9. Schematic representation of actinotrichia localization in fins at 3 dpa. (A) Regenerating stump of a caudal zebrafish fin at 3 days post amputation (dashed line). Lepidotrichia of the stump contain bone matrix (dark brown lines), whereas regenerating bones in the outgrowth consists of activated osteoblasts (light brown) with no or little bone matrix at this time point. Actinotrichia fibers (green) are oriented longitudinally to the proximo-distal axis in the new tissue (B) Transversal (cross) sections at different proximo-distal levels of the regenerate. (C) Longitudinal sections through ray and interray tissue. Actinotrichia are located between epidermis and mesenchyme in the distal-most blastema of the rays and in the entire distal blastema of the interrays. In the presence of regenerating bones in the rays, actinotrichia are displaced from their subepidermal position into the mesenchymal compartment where they become disrupted and misaligned in the proximal part of the regenerates.

trichia (Becerra et al., 1983; Geraudie, 1988; Geraudie and Landis, 1982; Geraudie and Meunier, 1982). Here, we aimed to determine the dynamics of actinotrichia in relation to lepidotrichia during the entire fin regenerative process in the zebrafish caudal fin. Using whole-mount analysis of transgenic fish with an osteoblast reporter, we visualized that actinotrichia are the first skeletal elements that become re-established in the regenerate before bone regrowth. This observation is consistent with previous studies performed on fin sections (Duran et al., 2011; Thorimbert et al., 2015; Zhang et al., 2010). Since in the intact adult fin, the actinotrichia form the apical skeleton of the appendage, their early re-establishment in the regenerative outgrowth can be viewed as a re-establishment of the distal-most positional identity at the onset of regeneration. According to this observation, the activation of cells of the stump may involve a switch of the positional value from proximal to distal. Based on this finding, we propose that the emerging blastema at least partially reproduces structural features of the intact fin margin. Moreover, the examination of fins at 3 dpa revealed that the early regenerative outgrowth contains actinotrichia across the entire new tissue, including interrays, revealing a similarity to the embryonic fin fold, which is uniformly supported with parallel fibers (Dane and Tucker, 1985; Geraudie, 1977; Thorogood, 1991; van den Boogaart et al., 2012; Wood and Thorogood, 1984; Zhang et al., 2010). This correlation suggests that the initiation of adult fin regeneration might at least partially recapitulate certain developmental processes used for extremity formation during embryogenesis.

The relationship between growth and pattern formation of a vertebrate limb is a long-standing question in developmental and regenerative biology (Bryant and Gardiner, 2016; Makanae et al., 2014; Marrero et al., 2017; McCusker et al., 2015; Mescher, 2017; Towers et al., 2012). Although the size of actinotrichia dynamically varied during regeneration, the whole-mount analysis revealed a strong morphometric and spatial complementarity between both skeletal structures – actinotrichia and lepidotrichia – throughout the entire regeneration process. The correlation between both skeletal elements was also observed in *another longfin* (*alf*^{dty86}) mutants, which contain irregular and long bony segments due to a gain-of-function mutation in the potassium channel *kcnk5b* (Perathoner et al., 2014). We showed that in addition to the defective lepidotrichia, the uninjured mutants displayed highly elongated actinotrichia. Moreover, the accelerated regeneration of *alf*^{dty86} mutant fins was also associated with markedly elongated actinotrichia. Interestingly, disrupted actinotrichia were reported in *alf*^{dty86} and in *short fin* (*sof*^{b123}) mutants during regeneration, probably due to alteration in the Connexin 43-dependent gene network (Bhadra and Iovine, 2015). It will be interesting to examine whether the phenotype is directly caused by the hyperpolarization of mutant cells or whether it arises as a secondary consequence of defective lepidotrichia.

The closer examination of longitudinal fin sections revealed that the epithelial-mesenchymal interface of the regenerating rays contains either actinotrichia or lepidotrichia-producing cells. The presence of osteoblasts was associated with a shift of actinotrichia from the subepithelial into the mesenchymal location. It is possible that regenerating osteoblasts actively change the configuration of pre-existing actinotrichia through a physical displacement and/or degradation of pre-existing fibers. Moreover, osteoblasts might affect actinotrichia at the level of gene expression, namely through suppression of *and1* in the lateral wound epithelium. In the fin, bone-forming cells are known to be tightly guided underneath of the basal wound epithelium (Quint et al., 2002; Smith et al., 2006; Stewart et al., 2014; Thorimbert et al., 2015; Zhang et al., 2012). The *and1* transcription was down-regulated in the epithelial cells adjacent to osteoblasts, and it extended further proximally in the interray than in the ray. This observation can be explained by a potential requirement for paracrine signals from the mesenchyme, such as Fgf20a and Activin-βA (Jazwinska et al., 2007; Whitehead et al., 2005), to induce *and1* expression in the overlying epithelium. A layer of bone-forming cells may form a barrier for the penetration of inductive signals from the mesenchyme. Indeed, regenerating osteoblasts are closely interconnected by N-cadherin-positive adherens junctions (Mateus et al., 2015), which might prevent diffusion of molecules between the overlying and underlying tissues. Thus, the layer of osteoblasts may physically interrupt epithelial-mesenchymal signaling and extracellular matrix-cell interactions that are required for the organization of actinotrichia.

The blocking of either TGFβ/Activin-βA or FGF signaling during the regenerative outgrowth phase inhibited not only *de-novo* synthesis of actinotrichia, but also impaired the maintenance of the pre-existing fibers. This finding supports previous observations of a high turnover of actinotrichia during regeneration (Mari-Beffa et al., 1989). In a similar experimental design, the inhibition of IGF signaling did not affect actinotrichia formation and maintenance, despite disrupting the regrowth process. This result indicates that the lack of actinotrichia formation after the inhibition of TGFβ/Activin-βA and FGF signaling are not merely side effects of the regenerative failure. This is consistent with previous studies, in which blocking of BMP signaling or Hdac1 impaired actinotrichia regeneration despite initiated dedifferentiation and partial outgrowth formation (Pfefferli et al., 2014; Thorimbert et al., 2015). Thus, actinotrichia deposition is not a default response to fin fold expansion, but it requires induction by signaling networks at the permissive epigenetic state of the cells. A recent study has reported an interesting approach to understanding the evolutionary and genetic principles of *and1* gene expression, using identification of tissue-specific *cis*-acting regulatory sequences of this gene (Lalonde et al., 2016). The characterization of essential enhancer elements of the *and1* gene opens a new perspective for studying the regulation of actinotrichia. The precise role of the signaling pathways, chromatin remodeling factors, matrix and cellular components during formation and turnover of actinotrichia provides a focus for future investigation.

4. Experimental procedures

4.1. Fish strains and fin amputations

For this study the following strains were used: AB strain (Oregon), *hsp70:dnfgfr1-egfp* (Lee et al., 2005), *dob* (*devoid of blastema*) (Whitehead et al., 2005), *osterix:nlsGFP* (*OlSp7:nlsGFP*^{zf132}) (Spoorendonk et al., 2008), *alf*^{dty86} (*another longfin*^{dty86}) (van Eeden et al., 1996). Adult fish were used at ages 12–36 months. For heat-shock experiments, the animals were placed in a water-bath regulated by a thermostat equipped with a cooling system (Lauda Eco), which was programed to increase the temperature from RT to 37 °C within 20 min, to maintain 37 °C for 1 h, and then to cool down to RT within 20 min. For fin amputation, fish were anesthetized in 0.6 mM tricaine (MS-222 ethyl-m-aminobenzoate, Sigma-Aldrich), and fins were amputated with a razor blade proximal to the first bone bifurcation point. Animals were kept at 27 °C for various durations before fin collection. Fins were fixed in 2% paraformaldehyde (PFA) overnight before subsequent procedures. Live images of regenerating fins were taken with a Leica AF M205 FA stereomicroscope. Animal experimentation was approved by the Cantonal Veterinary office of Fribourg, Switzerland.

4.2. Inhibitor treatments

Drug treatments were performed in 100 mL coplin jars (up to 3 fish per coplin jar). The following drugs were used: SB431542 (10 μM; Tocris), a TGFβ/Activin-βA receptor inhibitor; NVP-AEW541 (5 μM; Novartis Pharma AG), an IGF receptor inhibitor; PD173074 (10 μM; Selleckchem), an FGF receptor inhibitor. Drugs were dissolved in DMSO at 10 mM stock solution. Control fish were kept in 100 mL coplin jars containing 0.1% DMSO.

4.3. Immunofluorescence staining of fin sections

Fins were harvested at different time-points after amputation and fixed in 2% PFA in eppendorf tubes overnight at 4 °C. They were washed in PBS after fixation (3 × 10 min each) and transferred into Petri-dish containing a warm solution of 1.5% agarose/5% sucrose dissolved in water. After the gel solidified at RT, small blocks were cut around the embedded fins and equilibrated in 30% sucrose solution overnight at 4 °C. Then, the blocks were mounted in tissue freezing media (Tissue-Tek O.C.T.; Sakura), cryosectioned at 16 μm thickness using a Hyrax C50 cryostat, collected on Superfrost Plus slides (Fisher) and allowed to air dry for approx. 1 h at RT. Sections were stored in tight boxes at −20 °C for future use. Before use, slides were brought to room temperature for 10 min, the area with sections was encircled with ImmEdge Pen (Vector Laboratories) to keep liquid on the slides, and left for another 10 min at RT to dry. Then, the slides were transferred to Coplin jars containing 0.3% Triton-X in PBS (PBST) for 10 min at RT. The slides were transferred to a box lined with water-soaked paper towels to make a humid chamber. Blocking solution (5% goat serum in PBST) was applied on the sections for 1 h at RT. Subsequently, the sections were covered with approx. 200 μl of primary antibody diluted in blocking solution and incubated overnight at 4 °C in the humid chamber. They were washed in PBST in coplin jars for 1 h at RT and again transferred to the humid chamber for incubation with secondary antibodies diluted in blocking solution. The slides were washed in PBST for 1 h at RT and mounted in 90% glycerol in 20 mM Tris pH 8 with 0.5% N-propyl gallate.

The following primary antibodies were used: Rabbit anti-And1 (1:2000, custom-made against the C-terminus peptide of And1 CGQDDHLAYNGDYRKK, Eurogentec), Rat anti-And2 (1:10, custom-made against the C-terminus peptide of And2 CRFEDFLRAYMGGYKK, Eurogentec), Mouse Zns5 (1:250, Zebrafish International Resource Center), Mouse anti-α-Tubulin (1:1000, Sigma-Aldrich), Mouse anti-GM130 (1:200, BD Transduction Labs), Mouse IgM anti-chondroitin sulfate (1:2000, Sigma-Aldrich). Fluorescent dye-coupled secondary antibodies (Jackson Immunological) were used at 1:500 DAPI (Sigma-Aldrich) was used to label nuclei. Immunofluorescence and corresponding bright field were imaged using a Leica SP5 confocal microscope. Images were analyzed and processed using ImageJ and Adobe Photoshop. Imaris was used for movies and 3D projections.

4.4. Western blot

Western blots were performed on proteins of 3 dpa fin regenerates. Briefly, the regenerates from 20 fish were collected on dry ice, and homogenized in RIPA Lysis buffer (50 mM Tris–HCl pH = 8, 150 mM NaCl, 1% Triton X-100, Complete protease inhibitors (Roche)). Lysates were centrifuged to remove insoluble debris and the extracted soluble proteins were quantified with BCA kit against BSA standards, and denatured by boiling 5 min at 95 °C in sample buffer (final concentrations (1×): 12 mM Tris–HCl pH = 6.8, 2% SDS, 2% glycerol, 25 mM DTT). Serial dilutions of the soluble proteins (5, 15 and 45 μg) were loaded twice and resolved side-by-side onto one 8% SDS/PAGE gel. Proteins were transferred onto a 0.45 μm nitrocellulose membranes (GE Healthcare), which were then cut. After blocking in a 5% milk in TBST (1xTBS, 0.1% Tween-20) solution, one half membrane was incubated with Rabbit anti-And1 antibody (1:2000 in 5% milk-TBST) overnight; the second half membrane was incubated in Rat anti-And2 antibody (1:250 in 5% milk-TBST). The next day, both membranes were washed with TBST (3 × 10 min) and incubated with secondary antibodies: HRP anti-Rabbit (1:10,000 in 5% milk-TBST, Jackson Immunoresearch) and HRP anti-Rat (1:5000 in 5% milk-TBST, Thermo Scientific) respectively. After a second series of washes, the SuperSignal™ West Femto Maximum Sensitivity Substrate revelation kit (Thermo Scientific) was applied and chemiluminescence images were acquired using a Li-cor Odyssey reader. To allow visualization of the ladder, the bands were traced with a pen and imaged at 700 nm. Images of the two membranes were overlapped in Adobe photoshop.

4.5. Immunofluorescence staining of whole mount fins

Fins were harvested at different time-points after amputation and fixed in 2% PFA in eppendorf tubes overnight at 4 °C. They were washed in phosphate-buffered saline (PBS) after fixation, transferred to blocking solution containing 5% goat serum (Jackson Immunoresearch) in 0.3% Triton-X in PBS (PBST) for an hour at room temperature (RT). Then they were incubated in a primary antibody diluted in blocking solution overnight at 4 °C. On the next day, fins were washed in PBST (5 min, then 1 h) and incubated with a secondary antibody diluted in blocking solution for 2 h at room temperature. All the steps were done on a rocking platform. The fins were washed again and mounted in 90% glycerol in 20 mM Tris pH 8 with 0.5% N-propyl gallate (Sigma-Aldrich).

4.6. Morphometric analysis and statistics

The software ImageJ (NIH) was used for measurements of the regenerative outgrowth and actinotrichia length on projected Z-stacks of whole mount stainings. Each fin was represented by the average of the lengths obtained for the second, third and forth ray relative to the ventral and dorsal edges of the fin. Length of regenerates was measured by tracing and measuring a line from the amputation plane to the tip of the ray. Length of actinotrichia was measured by tracing a line from the most proximal And1-positive signal adjacent to a ray to the distal edge of the And1-positive signal. The values were then plotted in Graphpad prism. Student *T*-tests were performed comparing experimental groups to control group.

4.7. Histological staining of whole mount fins

Alcian Blue-Alizarin Red staining was performed according to previously published protocols (Laforest et al., 1998). Fins were fixed in 2% PFA and washed in PBS (3 × 10 min). The fins were first stained with Alcian Blue for 6 h (0.1% Alcian blue diluted in 30% acetic acid/70% ethanol and filtered). The fins were then dehydrated in a water-ethanol series (from 70% to 100% ethanol) and kept in ethanol at 4 °C overnight. On the next day, the fins were rehydrated in an ethanol-water series. They were then incubated 10 min at 37 °C in 0.5% trypsin in 2% sodium borate in water. After 5–6 rinses in water, they were then incubated 4 h in 0.1% Alizarin Red S in a 0.5% KOH solution for staining of bones. The fins were then transferred through a 0.5% KOH-glycerol series (up to 100% glycerol). The fins were left in glycerol overnight at 4 °C and mounted in glycerol. To avoid damaging the fins, all steps were performed in glass staining plates with shallow rounded wells.

4.8. Immunohistochemistry for electron microscopy

Distal fin regenerates were harvested at 3 dpa and fixed in 4% PFA overnight at 4 °C. They were washed in PBS (3 × 5 min each), embedded in warm solution of 1.5% agarose/5% sucrose dissolved in water. After agarose solidified at RT, small blocks with fins were cut and equilibrated in 30% sucrose solution overnight at 4 °C. Then, the blocks were embedded in tissue freezing media (TBS), cryosectioned at 80 μm thickness and collected in eppendorf tubes with PBS. The sections were blocked in 5% goat serum in PBS (GS/PBS) in PBS and incubated with Rabbit anti-And1 antibody diluted at 1:2000 in 5% GS/PBS at 4 °C overnight. The control sections were incubated with 5% GS/PBS without primary antibodies. On the next day, the sections were washed in PBS and incubated with Horse anti-Rabbit Biotinylated antibodies (Vector Laboratories) at 1:200 in GS/PBS for 2 h at room temperature. Then, the sections were washed in PBS and processed

using VECTASTAIN® ABC Kit (Vector Laboratories). The staining was performed using 3,3′-Diaminobenzidine (DAB) (Sigma-Aldrich) and H_2O_2 solution in Tris-buffered saline pH 7.6 solution. The sections were rinsed in PBS, fixed in 2% Glutaraldehyde in Cacodylate buffer, and processed for electron microscopy, according to the standard protocol.

4.9. In situ-hybridization

Primers for the generation of the template for the probes were as following:

and1 (NM_001197254): Fw 5′-caagacaggccttgaggaag-3′; Rev: 5′-gattgggaacttagtgggatgc-3′

and2 (NM_001111190): Fw 5′-cctgcagaacaagcacagag-3′; Rev: 5′-tggaactctgggagaactgg-3′

and3 (NM_001025511): Fw 5′-gtcacaggccacatctcttg-3′; Rev: 5′-atctgggagctctgatgacg-3′

and4 (NM_001136244): Fw 5′-tgtgtatgctgtccgtcctg-3′; Rev: 5′-gcgggtcgtagagttcagac-3′

To synthesize the anti-sense probes, a sequence of T3 RNA polymerase promoter (attaaccctcactaaagggaga) was added to the 5′ end of the reverse primers. The digoxigenin-RNA labeling mix (Roche) was used to generate the probe, which after purification was dissolved in hybridization solution and stored at −20 °C.

In-situ hybridization on whole fins and sections were performed as previously described (Chassot et al., 2016; Pfefferli and Jazwinska, 2017). Fin regenerates were fixed overnight at 4 °C in 4% PFA, then washed twice in PBS, once in PBS/methanol and in methanol for 10 min each, and finally transferred to methanol. Fixed fins were stored at −20 °C until processed for whole-mount *in-situ* hybridization or for cryosectioning.

For cryosectioning, fin regenerates were rehydrated in a methanol-PBS series and embedded using the same procedure as for immunofluorescence. Before use, slides were brought to room temperature for 10 min, and incubated in hybridization solution (50% formamide, 5 x SSC, 1 x Denhardt's solution, 10% dextran sulfate, 0.1 mg/mL yeast tRNA; all from Sigma-Aldrich) for 1 h at RT and for 1 h at 60 °C. Then, they were placed into tight boxes with wet paper towels, and 200 µl of diluted probe in hybridization solution (1:200) was applied on each slide that was then covered with a plastic coverslip (ApopTag, Merck Millipore) and placed in an incubator at 60 °C overnight. On the next day, slides were transferred to a coplin jar and soaked for 5 min with prewarmed 5 × SSC (Saline-sodium citrate) to allow the removal of cover slips, and washed twice with 5 × SSC for 30 min and once with 0.2 × SSC for 1 h, each step at 60 °C. The final wash was done with 0.2 × SSC for 5 min at RT. Slides were allowed to dry for a few minutes at RT and the area with sections was encircled with the ImmEdge Pen, and left for 15 min for drying. The slides were placed into humidified boxes, and 1× blocking reagent solution (Roche) in maleic acid buffer (100 mM Maleic Acid, 150 mM NaCl, 0.2% Tween-20, pH 7.5; all from Sigma-Aldrich) was applied on the sections for 1 h at RT. Subsequently, 250 µl of anti-dig-alkaline phosphatase (AP) antibody (Roche; diluted 1:4000 in blocking reagent solution) was applied on the sections for 2 h at RT. The slides were rinsed and washed twice for 30 min in maleic acid buffer in coplin jars. Then, the slides were washed twice in AP-buffer (100 mM Tris HCL pH 9.5, 100 mM NaCl, 50 mM MgCl2, and 0.2% Tween 20) for 5 min. To prepare the staining reagents, NBT and BCIP compounds (Roche) were diluted in AP-buffer according to manufacturer's instruction with addition of 10% Polyvinyl alcohol (Sigma-Aldrich). The staining reaction was performed in a humidified box at 37 °C. The reaction was monitored under the microscope, and was stopped by washes in coplin jars with PBS for 15 min, 70% ethanol for 1 h, and 15 min in PBS. The slides were mounted in Aquatex mounting medium (Merck Millipore).

For the fins of transgenic *osterix(sp7):nlsEGFP* fish, after completion of *in-situ* hybridization, we continued with the standard immunofluoresce staining using chicken antibodies against GFP at 1:1000 (GFP-1010, Aves Labs). Immunofluorescence and corresponding bright field images were taken using a Leica SP5 confocal microscope and a Zeiss microscope, respectively, and were superimposed using Adobe Photoshop.

4.10. Quantitative gene expression analyses

Quantitative RT-PCR reactions were performed as previously described (Chablais and Jazwinska, 2010). The values were normalized for *β-actin*. The expression ratios were calculated using the Pfaffl method. The following primers were used:

and1: Fw 5′-ccgaacccgtcagtatttcc-3′; Rev: 5′-gcgtcatattgctgctggtc-3′

β-actin: Fw 5′-ttggcaatgagaggttcagg-3′; Rev 5′-tggagtt-gaaggtggtctcg-3′

Acknowledgement

We are grateful to Prof. Marco Celio (Department of Medicine, University of Fribourg), in whose lab this work was started. Special thanks to B. Scolari for electron microscopy imaging, S. Käser-Pébernard for help with the Western blot, V. Zimmermann for technical help, C. Pfefferli for critical reading of the manuscript, F. Hofmann, Novartis Pharma AG for providing NVP-AEW541, C. Bono Mestre and F. Chablais and V. Thorimbert for experimental contribution. This work was supported by the Swiss National Science Foundation, grant numbers: 310030_159995 and CRSII3_147675.

Competing interest

The authors declare no financial or non-financial competing interests.

Appendix A. Supporting information

Supplementary data associated with this article can be found in the online version at doi:10.1016/j.ydbio.2017.07.024.

References

Akimenko, M.A., Mari-Beffa, M., Becerra, J., Geraudie, J., 2003. Old questions, new tools, and some answers to the mystery of fin regeneration. Dev. Dyn. 226, 190–201.
Armstrong, B.E., Henner, A., Stewart, S., Stankunas, K., 2017. Shh promotes direct interactions between epidermal cells and osteoblast progenitors to shape regenerated zebrafish bone. Development 144, 1165–1176.
Becerra, J., Junqueira, L.C., Bechara, I.J., Montes, G.S., 1996. Regeneration of fin rays in teleosts: a histochemical, radioautographic, and ultrastructural study. Arch. Histol. Cytol. 59, 15–35.
Becerra, J., Montes, G.S., Bexiga, S.R., Junqueira, L.C., 1983. Structure of the tail fin in teleosts. Cell Tissue Res. 230, 127–137.
Bechara, J., Böckelmann, P., Santiago Montes, G., da Cruz-Höfling, M.A., 2003. Inhibiiton of caudal fin actinotrichia regeneration by acetylsalicylic acid (Aspirin) in teleosts. Braz. J. Morphol. Sci. 20, 67–74.
Bhadra, J., Iovine, M.K., 2015. Hsp47 mediates Cx43-dependent skeletal growth and patterning in the regenerating fin. Mech. Dev. 138 (Pt 3), 364–374.
Birk, D.E., Brückner, P., 2011. Collagens, Suprastructures, and Collagen Fibril Assembly. In: Mecham, R.P. (Ed.), The Extracellular Matrix: an Overview. Springer-Verlag Berlin Heidelberg, Berlin Heidelberg, 77–115.
Blum, N., Begemann, G., 2015. Osteoblast de- and redifferentiation are controlled by a dynamic response to retinoic acid during zebrafish fin regeneration. Development 142, 2894–2903.
Brown, A.M., Fisher, S., Iovine, M.K., 2009. Osteoblast maturation occurs in overlapping proximal-distal compartments during fin regeneration in zebrafish. Dev. Dyn. 238, 2922–2928.
Bryant, S.V., Gardiner, D.M., 2016. The relationship between growth and pattern formation. Regeneration.
Chablais, F., Jazwinska, A., 2010. IGF signaling between blastema and wound epidermis is required for fin regeneration. Development 137, 871–879.
Chassot, B., Pury, D., Jazwinska, A., 2016. Zebrafish fin regeneration after cryoinjury-induced tissue damage. Biol. Open 5, 819–828.
Dane, P.J., Tucker, J.B., 1985. Modulation of epidermal-cell shaping and extracellular-matrix during caudal fin morphogenesis in the zebra fish Brachydanio-rerio. J. Embryol. Exp. Morphol. 87, 145–161.

Duran, I., Csukasi, F., Taylor, S.P., Krakow, D., Becerra, J., Bombarely, A., Mari-Beffa, M., 2015. Collagen duplicate genes of bone and cartilage participate during regeneration of zebrafish fin skeleton. Gene Expr. Patterns 19, 60–69.
Duran, I., Mari-Beffa, M., Santamaria, J.A., Becerra, J., Santos-Ruiz, L., 2011. Actinotrichia collagens and their role in fin formation. Dev. Biol. 354, 160–172.
Feitosa, N.M., Zhang, J., Carney, T.J., Metzger, M., Korzh, V., Bloch, W., Hammerschmidt, M., 2012. Hemicentin 2 and Fibulin 1 are required for epidermal-dermal junction formation and fin mesenchymal cell migration during zebrafish development. Dev. Biol. 369, 235–248.
Galloway, J., 1985. Elastoidin. In: Bairati, Aa.G., R. (Ed.), Biology of Invertebrate and Lower Vertebrate Collagens. Plenum Press, New York and London.
Geraudie, J., 1977. Initiation of the actinotrichial development in the early fin bud of the fish, Salmo. J. Morphol. 151, 353–361.
Geraudie, J., 1988. Fine structural peculiarities of the pectoral fin dermoskeleton of two brachiopterygii, Polypterus senegalus and Calamoichthys calabaricus (Pisces, Osteichthyes). Anat. Rec. 221, 455–468.
Geraudie, J., Landis, W.J., 1982. The fine structure of the developing pelvic fin dermal skeleton in the trout Salmo gairdneri. Am. J. Anat. 163, 141–156.
Geraudie, J., Meunier, F.J., 1980. Elastoidin actinotrichia in Coelacanth fins: a comparison with teleosts. Tissue Cell 12, 637–645.
Geraudie, J., Meunier, F.J., 1982. Comparative fine structure of the Osteichthyan dermotrichia. Anat. Rec. 202, 325–328.
Govindan, J., Iovine, M.K., 2014. Hapln1a is required for connexin43-dependent growth and patterning in the regenerating fin skeleton. PLoS One 9, e88574.
Govindan, J., Iovine, M.K., 2015. Dynamic remodeling of the extra cellular matrix during zebrafish fin regeneration. Gene Expr. Patterns 19, 21–29.
Grandel, H., Schulte-Merker, S., 1998. The development of the paired fins in the zebrafish (Danio rerio). Mech. Dev. 79, 99–120.
Heude, E., Shaikho, S., Ekker, M., 2014. The dlx5a/dlx6a genes play essential roles in the early development of zebrafish median fin and pectoral structures. PLoS One 9, e98505.
Huang, C.C., Wang, T.C., Lin, B.H., Wang, Y.W., Johnson, S.L., Yu, J., 2009. Collagen IX is required for the integrity of collagen II fibrils and the regulation of vascular plexus formation in zebrafish caudal fins. Dev. Biol. 332, 360–370.
Hulmes, D.J.S., Wess, T.J., Prockop, D.J., Fratzl, P., 1995. Radial packing, order, and disorder in collagen fibrils. Biophys. J. 68, 1661–1670.
Jazwinska, A., Badakov, R., Keating, M.T., 2007. Activin-betaA signaling is required for zebrafish fin regeneration. Curr. Biol. 17, 1390–1395.
Jazwinska, A., Sallin, P., 2016. Regeneration versus scarring in vertebrate appendages and heart. J. Pathol. 238, 233–246.
Kemp, N.E., Park, J.H., 1970. Regeneration of lepidotrichia and actinotrichia in the tailfin of the teleost Tilapia mossambica. Dev. Biol. 22, 321–342.
Knopf, F., Hammond, C., Chekuru, A., Kurth, T., Hans, S., Weber, C.W., Mahatma, G., Fisher, S., Brand, M., Schulte-Merker, S., Weidinger, G., 2011. Bone regenerates via dedifferentiation of osteoblasts in the zebrafish fin. Dev. Cell 20, 713–724.
Laforest, L., Brown, C.W., Poleo, G., Geraudie, J., Tada, M., Ekker, M., Akimenko, M.A., 1998. Involvement of the sonic hedgehog, patched 1 and bmp2 genes in patterning of the zebrafish dermal fin rays. Development 125, 4175–4184.
Lalonde, R.L., Moses, D., Zhang, J., Cornell, N., Ekker, M., Akimenko, M.A., 2016. Differential actinodin1 regulation in zebrafish and mouse appendages. Dev. Biol. 417, 91–103.
Lee, Y., Grill, S., Sanchez, A., Murphy-Ryan, M., Poss, K.D., 2005. Fgf signaling instructs position-dependent growth rate during zebrafish fin regeneration. Development 132, 5173–5183.
Makanae, A., Mitogawa, K., Satoh, A., 2014. Implication of two different regeneration systems in limb regeneration. Regeneration 1, 1–9.
Mari-Beffa, M., Carmona, M.C., Becerra, J., 1989. Elastoidin turn-over during tail fin regeneration in teleosts. A morphometric and radioautographic study. Anat. Embryol. 180, 465–470.
Mari-Beffa, M., Murciano, C., 2010. Dermoskeleton morphogenesis in zebrafish fins. Dev. Dyn. 239, 2779–2794.
Marrero, L., Simkin, J., Sammarco, M., Muneoka, K., 2017. Fibroblast reticular cells engineer a blastema extracellular network during digit tip regeneration in mice. Regeneration 4, 69–84.
Mateus, R., Lourenco, R., Fang, Y., Brito, G., Farinho, A., Valerio, F., Jacinto, A., 2015. Control of tissue growth by Yap relies on cell density and F-actin in zebrafish fin regeneration. Development 142, 2752–2763.
McCusker, C., Bryant, S.V., Gardiner, D.M., 2015. The axolotl limb blastema: cellular and molecular mechanisms driving blastema formation and limb regeneration in tetrapods. Regeneration 2, 54–71.
Mescher, A.L., 2017. Macrophages and fibroblasts during inflammation and tissue repair in models of organ regeneration. Regeneration 4, 39–53.
Montes, G.S., Becerra, J., Toledo, O.M., Gordilho, M.A., Junqueira, L.C., 1982. Fine structure and histochemistry of the tail fin ray in teleosts. Histochemistry 75, 363–376.
Nolte, H., Holper, S., Housley, M.P., Islam, S., Piller, T., Konzer, A., Stainier, D.Y., Braun, T., Kruger, M., 2015. Dynamics of zebrafish fin regeneration using a pulsed SILAC approach. Proteomics 15, 739–751.
Perathoner, S., Daane, J.M., Henrion, U., Seebohm, G., Higdon, C.W., Johnson, S.L., Nusslein-Volhard, C., Harris, M.P., 2014. Bioelectric signaling regulates size in zebrafish fins. PLoS Genet. 10, e1004080.
Pfefferli, C., Jazwinska, A., 2017. The careg element reveals a common regulation of regeneration in the zebrafish myocardium and fin. Nat. Commun. 8, 15151.
Pfefferli, C., Jaźwińska, A., 2015. The art of fin regeneration in zebrafish. Regeneration 2, 72–83.
Pfefferli, C., Muller, F., Jazwinska, A., Wicky, C., 2014. Specific NuRD components are required for fin regeneration in zebrafish. BMC Biol. 12, 30.
Poss, K.D., Shen, J., Nechiporuk, A., McMahon, G., Thisse, B., Thisse, C., Keating, M.T., 2000. Roles for Fgf signaling during zebrafish fin regeneration. Dev. Biol. 222, 347–358.
Quint, E., Smith, A., Avaron, F., Laforest, L., Miles, J., Gaffield, W., Akimenko, M.A., 2002. Bone patterning is altered in the regenerating zebrafish caudal fin after ectopic expression of sonic hedgehog and bmp2b or exposure to cyclopamine. Proc. Natl. Acad. Sci. USA 99, 8713–8718.
Smith, A., Avaron, F., Guay, D., Padhi, B.K., Akimenko, M.A., 2006. Inhibition of BMP signaling during zebrafish fin regeneration disrupts fin growth and scleroblasts differentiation and function. Dev. Biol. 299, 438–454.
Sordino, P., Vanderhoeven, F., Duboule, D., 1995. Hox gene-expression in teleost fins and the origin of vertebrate digits. Nature 375, 678–681.
Sousa, S., Afonso, N., Bensimon-Brito, A., Fonseca, M., Simoes, M., Leon, J., Roehl, H., Cancela, M.L., Jacinto, A., 2011. Differentiated skeletal cells contribute to blastema formation during zebrafish fin regeneration. Development 138, 3897–3905.
Spoorendonk, K.M., Peterson-Maduro, J., Renn, J., Trowe, T., Kranenbarg, S., Winkler, C., Schulte-Merker, S., 2008. Retinoic acid and Cyp26b1 are critical regulators of osteogenesis in the axial skeleton. Development 135, 3765–3774.
Stewart, S., Gomez, A.W., Armstrong, B.E., Henner, A., Stankunas, K., 2014. Sequential and opposing activities of Wnt and BMP coordinate zebrafish bone regeneration. Cell Rep. 6, 482–498.
Stewart, S., Stankunas, K., 2012. Limited dedifferentiation provides replacement tissue during zebrafish fin regeneration. Dev. Biol. 365, 339–349.
Thorimbert, V., Konig, D., Marro, J., Ruggiero, F., Jazwinska, A., 2015. Bone morphogenetic protein signaling promotes morphogenesis of blood vessels, wound epidermis, and actinotrichia during fin regeneration in zebrafish. FASEB J. 29, 4299–4312.
Thorogood, P., 1991. The Development of the Teleost Fin and Implications for our Understanding of Tetrapod Lim Evolution. In: Hinchliffe, J.R. (Ed.), Developmental Patterning of the Vertebrate Limb. Springer Science+Business Media, New York, 347–354.
Tornini, V.A., Poss, K.D., 2014. Keeping at arm's length during regeneration. Dev. Cell 29, 139–145.
Towers, M., Wolpert, L., Tickle, C., 2012. Gradients of signalling in the developing limb. Curr. Opin. Cell Biol. 24, 181–187.
Tu, S., Johnson, S.L., 2011. Fate restriction in the growing and regenerating zebrafish fin. Dev. Cell 20, 725–732.
van den Boogaart, J.G., Muller, M., Osse, J.W., 2012. Structure and function of the median finfold in larval teleosts. J. Exp. Biol. 215, 2359–2368.
van Eeden, F.J., Granato, M., Schach, U., Brand, M., Furutani-Seiki, M., Haffter, P., Hammerschmidt, M., Heisenberg, C.P., Jiang, Y.J., Kane, D.A., Kelsh, R.N., Mullins, M.C., Odenthal, J., Warga, R.M., Nusslein-Volhard, C., 1996. Genetic analysis of fin formation in the zebrafish, Danio rerio. Development 123, 255–262.
Wehner, D., Cizelsky, W., Vasudevaro, M.D., Ozhan, G., Haase, C., Kagermeier-Schenk, B., Roder, A., Dorsky, R.I., Moro, E., Argenton, F., Kuhl, M., Weidinger, G., 2014. Wnt/beta-catenin signaling defines organizing centers that orchestrate growth and differentiation of the regenerating zebrafish caudal fin. Cell Rep. 6, 467–481.
Wehner, D., Weidinger, G., 2015. Signaling networks organizing regenerative growth of the zebrafish fin. Trends Genet. 31, 336–343.
Whitehead, G.G., Makino, S., Lien, C.L., Keating, M.T., 2005. fgf20 is essential for initiating zebrafish fin regeneration. Science 310, 1957–1960.
Witten, P.E., Huysseune, A., 2007. Mechanisms of Chondrogenesis and Osteogenesis in Fins. In: Hall, B.K. (Ed.), Fins into Limbs. Evolution, Development and Transformation. The University of Chicago Press, Chicago and London, 79–92.
Wood, A., Thorogood, P., 1984. An analysis of in vivo cell migration during teleost fin morphogenesis. J. Cell Sci. 66, 205–222.
Wood, A., Thorogood, P., 1987. An ultrastructural and morphometric analysis of an invivo contact guidance-system. Development 101, 363–381.
Zhang, J., Jeradi, S., Strahle, U., Akimenko, M.A., 2012. Laser ablation of the sonic hedgehog-a-expressing cells during fin regeneration affects ray branching morphogenesis. Dev. Biol. 365, 424–433.
Zhang, J., Wagh, P., Guay, D., Sanchez-Pulido, L., Padhi, B.K., Korzh, V., Andrade-Navarro, M.A., Akimenko, M.A., 2010. Loss of fish actinotrichia proteins and the fin-to-limb transition. Nature 466, 234–237.